Published online May 24, 2018

Original Research

Core Ideas

- We present a semiautomated framework for large-scale calibration of capacitance soil moisture sensors.
- Soil-specific calibrations are needed for accurate moisture measurements in nearly all soil types.
- Transparent, traceable, and complete uncertainty estimates provided for entire approach.

A Robust Calibration Method for Continental-Scale Soil Water Content Measurements

Joshua A. Roberti,* Edward Ayres, Henry W. Loescher, Jianwu Tang, Gregory Starr, David J. Durden, Derek E. Smith, Elizabeth de la Reguera, Kate Morkeski, Margot McKlveen, Heidi Benstead, Michael D. SanClements, Robert H. Lee, Maheteme Gebremedhin, and Rommel C. Zulueta

Technological advances have allowed in situ monitoring of soil water content in an automated manner. These advances, along with an increase in large-scale networks monitoring soil water content, stress the need for a robust calibration framework that ensures that soil water content measurements are accurate and reliable. We have developed an approach to make consistent and comparable soil water content sensor calibrations across a continental-scale network in a production framework that incorporates a thorough accounting of uncertainties. More than 150 soil blocks of varying characteristics from 33 locations across the United States were used to generate soil-specific calibration coefficients for a capacitance sensor. We found that the manufacturer's nominal calibration coefficients poorly fit the data for nearly all soil types. This resulted in negative (91% of samples) and positive (5% of samples) biases and a mean root mean square error (RMSE) of 0.123 $cm^3\ cm^{-3}$ (1σ) relative to reference standard measurements. We derived soil-specific coefficients, and when used with the manufacturer's nominal function, the biases were corrected and the mean RMSE dropped to $\pm 0.017\ cm^3\ cm^{-3}$ ($\pm 1\sigma$). A logistic calibration function further reduced the mean RMSE to $\pm 0.016\ cm^3\ cm^{-3}$ ($\pm 1\sigma$) and increased the range of soil moistures to which the calibration applied by 18% compared with the manufacturer's function. However, the uncertainty of the reference standard was notable ($\pm 0.022\ cm^3\ cm^{-3}$), and when propagated in quadrature with RMSE estimates, the combined uncertainty of the calibrated volumetric soil water content values increased to $\pm 0.028\ cm^3\ cm^{-3}$ regardless of the calibration function used.

Abbreviations: DPHP, dual-pulse heat probe; FDR, frequency-domain reflectometry; NEON, National Ecological Observatory Network; NMM, neutron moisture meter; NSF, National Science Foundation; PRT, platinum resistance thermometer; RMSE, root mean square error; TDR, time-domain reflectometry.

J.A. Roberti, E. Ayres, H.W. Loescher, D.J. Durden, M.D. SanClements, R.H. Lee, and R.C. Zulueta, National Ecological Observatory Network, Boulder, CO 80301; H.W. Loescher and M.D. SanClements, Institute of Arctic and Alpine Research, Univ. of Colorado, Boulder, CO 80303; J. Tang, E. de la Reguera, K. Morkeski, and M. McKlveen, Ecosystems Center, Marine Biological Lab., Woods Hole, MA 02543; G. Starr and H. Benstead, Dep. of Biological Sciences, Univ. of Alabama, Tuscaloosa, AL 35487; D.E. Smith, Univ. of Colorado Cancer Center, Univ. of Colorado, Aurora, CO 80045; M. Gebremedhin, Dep. of Environmental Studies and Sustainable Systems, Kentucky State Univ., Frankfort, KY 40601. *Corresponding author (jroberti@BattelleEcology.org).

Received 2 Oct. 2017.
Accepted 4 Apr. 2018.
Supplemental material online.

Citation: Roberti, J.A., E. Ayres, H.W. Loescher, J. Tang, G. Starr, D.J. Durden, D.E. Smith, E. de la Reguera, K. Morkeski, M. McKlveen, H. Benstead, M.D. SanClements, R.H. Lee, M. Gebremedhin, and R.C. Zulueta. 2018. A robust calibration method for continental-scale soil water content measurements. Vadose Zone J. 17:170177. doi:10.2136/vzj2017.10.0177

Soil moisture is an important driver of numerous biogeophysical processes at scales ranging from the aggregate to the globe. The vertical and lateral flow of water through the soil determines patterns of eluviation and illuviation, making them central to soil pedogenesis, and control the flux of solutes within the soil profile and across the terrestrial aquatic interface, with implications for the transport of nutrients and pollutants (Kaiser et al., 2004) including dissolved organic matter (Burns et al., 2016; Kalbitz et al., 2000). Dissolved organic matter is a significant component of the global C budget, and the flux of dissolved organic matter within soils and into water bodies has implications for the global C cycle (Battin et al., 2008). Additionally, soil moisture status is important for the decomposition of soil organic matter and the form in which C is respired (e.g., CO_2 or CH_4) (Davidson et al. 2008). Soil moisture is also a determinant of ecosystem structure, sensible and latent heat fluxes, water balance, and local climate (Koster et al., 2004; IPCC, 2007; Stanford and Epstein, 1974).

Soil moisture evolves along a continuum of water availability from saturation to the permanent wilting point, with the range following the loss of gravitational water (i.e., field

capacity) to a water potential of approximately −1500 kPa (i.e., the permanent wilting point) representing plant-available water. Soil is considered to be saturated if all the pores within the soil are filled with water. If no additional water is added to the soil, the soil surface will begin to dry. Simultaneously yet independently, water will also begin to percolate out of the larger soil pores under gravity until field capacity is reached; this process usually takes only a few hours for sandy soils but can take up to 72 h for soils with a high clay content (Weil and Brady, 2017). Once field capacity is reached, further drying of the soil is slow and becomes a function of evaporation and transpiration stages. In the first stage, the flow of capillary water (the water in small pores of the soil) to the soil surface is sufficient to meet the demand of the evaporative rate of the ambient atmosphere (Lemon, 1956). In the second stage, vapor movement replaces capillary flow as the dominant transport mechanism, and the rate of soil drying decreases (Idso et al., 1974). If the soil is vegetated, plants will also contribute to the drying of soils by removing water from their rooting zone (Weil and Brady, 2017). As the soil continues to dry, the remaining water molecules are more tightly held within the soil matrix, which makes it harder for plants to extract water (Campbell and Norman, 1998). Eventually, soil moisture levels reach the wilting point, the amount of water retained by the soil when the water potential is approximately −1500 kPa.

Direct estimates of soil water content are made by sampling a known volume of soil, weighing it before and after oven drying, and calculating the difference in weight, i.e., the gravimetric approach (Gardner, 1986). While the gravimetric approach respects first principles and is considered the standard against which other soil water content methods are compared (Gardner et al., 2001), it cannot be performed in a nondestructive manner, nor can a continuous time series be estimated across a range of moisture contents. Studies that seek to quantify continuous volumetric soil water content (θ_v) must rely on automated instrumentation. An abundance of in situ and remote sensing technologies allow the automated monitoring of θ_v at different spatial and temporal scales. The applicability of each measurement system is directly related to the underlying goals of the project. Measurements of θ_v at the point scale (<1 m^2) are commonly obtained by the neutron moisture meter (NMM), dual-pulse heat probe (DPHP), and an array of electromagnetic technologies. Most of these methods allow continuous (e.g., sub-hourly) monitoring of θ_v. Remote sensing platforms, such as passive and active satellites, are used to quantify θ_v at larger spatial scales (≥3 km^2) and temporal scales (e.g., daily to weekly). An overview of in situ technologies is presented below.

Neutron moisture meters emit neutrons (radioactive material) into the surrounding soil environment. A linear relationship exists between the count ratio of neutrons and θ_v, which makes NMMs easy to calibrate. It is possible to calibrate these sensors to a RMSE of <0.01 $cm^3\ cm^{-3}$ (Evett and Steiner, 1995), and because of this NMMs are considered to be the most accurate sensor-based method for quantifying θ_v (International Atomic Energy Agency, 2008). However, because of the risks associated with their radioactive source, NMM usage is declining (Hillel, 1998).

Heat pulse sensors measure soil volumetric heat capacity by emitting a short heat pulse from one probe and measuring the temperature response at the second probe; the volumetric heat capacity is directly related to θ_v (Ochsner et al., 2003). Studies have noted that calibrated DPHPs can provide estimates of absolute θ_v with accuracies ranging between ±0.02 and ±0.05 $cm^3\ cm^{-3}$ (e.g., Heitman et al., 2003; Ren et al., 2003). Dual-pulse heat probes are relatively low cost and are insensitive to salinity (Ren et al., 2000), which makes them an attractive option for θ_v monitoring. However, these sensors show high sensitivity to the geometrical configuration of the probes and soil constituents, which introduces measurement inaccuracies (Robinson et al., 2003). Additionally, the accuracy of DPHP measurements has been reported to degrade with time, thus hinting that DPHPs are more appropriate for quantifying changes in θ_v rather than quantifying absolute quantities of θ_v (Basinger et al., 2003).

Many sensor technologies come under the electromagnetic umbrella. These include but are not limited to time-domain reflectometry (TDR) and frequency domain reflectometry (FDR). Broadly speaking, the measurement theories of TDR and FDR are similar. Electromagnetic pulses emanated by the sensor are used to quantify the dielectric constant of the soil surrounding the sensor (Rundel and Jarrell, 1989). The dielectric constant is the ratio of the dielectric of the material, e.g., soil, to the dielectric of a vacuum and describes the material's ability to store electrical energy (Bosch, 2004). The dielectric constants of water at 20°C, dry soil, and air are 80, 4.5 to 10, and 1, respectively (Robinson et al., 2003). Because of these large differences in dielectric constants, θ_v can be discerned from changes in the dielectric constant of the soil volume being sampled (Bosch, 2004). Time-domain reflectometry sensors commonly operate at a fixed frequency between 0.5 and 1.0 GHz, while FDR sensors (i.e., capacitance and impedance probes) operate at a single frequency or in a narrow band of frequencies between 0.05 and 0.15 GHz (Gardner et al., 1998). Soil-specific calibrations of TDR sensors and capacitance probes have been shown to improve the accuracies of θ_v estimates. Across a range of moisture contents and soil types, TDRs have been calibrated to accuracies of ±0.014 to ±0.025 $cm^3\ cm^{-3}$ (Blonquist et al., 2005; Robinson et al., 2008), ±0.021 to ±0.046 $cm^3\ cm^{-3}$ (Weitz et al., 1997), and ±0.006 to ±0.019 $cm^3\ cm^{-3}$ (International Atomic Energy Agency, 2008), while FDR sensors have achieved accuracies of ±0.014 to ±0.032 $cm^3\ cm^{-3}$ (Baumhardt et al., 2000), ±0.015 to ±0.078 $cm^3\ cm^{-3}$ (Sharma et al., 2017), ±0.05 $cm^3\ cm^{-3}$ (Bosch, 2004), and ±0.033 to ±0.055 $cm^3\ cm^{-3}$ (Rowlandson et al., 2013). The lower operational frequencies of the capacitance and impedance probes are sensitive to salinity (electrical conductivity), temperature, high-charge clays, and organic matter, which can affect the accuracy of θ_v estimates (Bosch, 2004; Baumhardt et al., 2000; Logsdon, 2009; Seyfried and Murdock, 2004).

Despite the abundance of available technology, measurements of soil moisture are often lacking at the intermediate

scale (0.1–1 km^2) (Entekhabi et al., 2010; Robinson et al., 2008; Seneviratne et al., 2010). Gaps in our understanding of soil moisture and related processes exist at this scale as a result of measurement constraints at the sample scale (100–1000 cm^3) and at the soil surface at large spatial scales using remote sensing (Western et al., 2002). In the last few decades, a handful of platforms have emerged that help bridge this intermediate spatial gap. These platforms, such as the COsmic-ray Soil Moisture Observing System (COSMOS), the Soil Moisture Active Passive (SMAP) Mission, the Soil Climate Analysis Network (SCAN), Snow Telemetry (SNOTEL) network, and the US Climate Reference Network (USCRN) play an integral role in intermediate-scale soil moisture monitoring and provide invaluable data that help inform drought assessment, water resource management, and climate modeling (Ardekani, 2013; Bell et al., 2013; Huisman et al., 2001; Schaefer et al., 2007). Collectively, these platforms monitor soil moisture at slightly different depths, spatial scales, and temporal resolutions, thus mitigating the lack of quality data at the intermediate scale denoted by Western et al. (2002). Advances in sensor technology and the advent of additional large-scale distributed observatories such as the National Ecological Observatory Network (NEON) provide further opportunities to complement these existing networks by linking multiple point observations with regional processes and responses at the intermediate scale (0.1–1 km^2). The ability to accomplish this in a feasible manner is the next big challenge for large-scale networks (Robinson et al., 2008).

In 2004, the National Science Foundation (NSF) sponsored several workshops to determine the scientific requirements to inform the observational design and methods (e.g., sensor-based technology) of future large-scale ecological networks. The workshops pinpointed several key issues for consideration. These included sensor robustness (reliable and rugged with low power requirements), in situ calibration needs (resistant to degradation and signal drift), ease of maintenance during the network's projected lifespan, and network design strategies (sufficient coverage at least cost) (World Technology Evaluation Center, 2004). Specific to soil moisture, recommendations included that measurements be made (i) continuously up to 2 m deep, (ii) at five soil plots per site, (iii) consistently over decadal time periods, (iv) such that the sensors can be retrievable to allow for regular calibration and maintenance, and (v) with a level of accuracy needed for large-scale ecological and hydrological studies (e.g., Entekhabi et al., 2010; International Atomic Energy Agency, 2008; Kerr et al., 2010; Robinson et al., 2008).

The limitations of some techniques and the guidance from the NSF workshops narrowed down the θ_v measurement technologies applicable for the NEON project. Remote sensing platforms do not provide the necessary spatial resolution (horizontal and depth) or temporal resolution necessary for monitoring of θ_v to fit the goals of NEON. Neutron moisture meters are appropriate for measuring θ_v at the intermediate scales but they are considered not practical due to health risks. Both DPHP and TDR require direct contact with the soil and must be permanently buried in the soil, whereas capacitance probes are typically installed via an access tube, which leaves them accessible for future maintenance, a major advantage of capacitance probes. Because of the latter and the ability to meet the other criteria outlined by the NSF, capacitance probes were deemed the most feasible method for the scope of the NEON project.

It is well known that soil-specific calibrations are necessary to ensure accurate θ_v estimates using capacitance probes (e.g., Bosch, 2004; Baumhardt et al., 2000; Cosh et al., 2016). This is especially important for distributed sensor networks such as NEON that span a wide range of soil types. However, information pertaining to calibrations of capacitance probes for use in a large-scale observatory are lacking. This information gap, along with the increasing number of ecological networks providing data to the scientific community (see Chabbi et al., 2017; Loescher et al., 2017) and the advent of more comparative studies involving cross-site, cross-ecosystem, and novel scaling approaches, stress the need for a robust and standardized calibration framework that ensures that accurate and precise θ_v estimates are obtained in a traceable and transparent manner. Here we describe the methodology for robust calibrations of a capacitance probe, including a transparent and traceable uncertainty analysis for the entire method and resulting measurements. More specifically, we describe a novel large-scale approach toward soil-specific sensor calibrations that includes: (i) application of methods across soil horizons and sites to provide consistent and comparable data across continental-scale networks; (ii) creation of a workflow that allows calibration coefficients to be generated in a semi-automated production (laboratory) setting; and (iii) a thorough accounting of uncertainties at each stage of the calibration process.

Methods

Sensor Selection

During NEON's sensor selection process, a capacitance sensor, the EnviroSCAN TriSCAN (Sentek Pty.), was chosen because of its ability to meet the evaluated recommendations provided by the NSF. The EnviroSCAN operates at frequencies between 48 and 75 MHz in deionized water and air, respectively (International Atomic Energy Agency, 2008). The sensor outputs a scaled frequency (normalized between 0 and 1) that varies proportionally with soil permittivity (dielectric constant) and increasing water content (Baumhardt et al., 2000). According to the manufacturer, the EnviroSCAN integrates its measurements over a volume of soil that extends 5 cm above and below the vertical midpoint of the sensor and 14 cm horizontally from the edge of the access tube (Sentek, 2011). Studies conducted by Evett and Cepuder (2008) and Paltineanu and Starr (1997), however, found that θ_v measured by the EnviroSCAN is primarily influenced by the soil within a few centimeters of the sensor, with ~90% of the signal detected from the soil within 4 cm of the access tube. The EnviroSCAN was found to be sensitive to temperature fluctuations and salinity, the latter resulting in measurements of θ_v exceeding the available pore space of the soil (Baumhardt et al., 2000).

Soil Sample Collection

The soil water content calibrations presented here were generated from samples collected at soil pits from 33 terrestrial NEON

sites (Fig. 1). A small excavator was used to dig the soil pit at each site. To minimize disturbance to the site and soil, the excavator was limited to a defined access route to and from the soil pit. Each soil pit was approximately 2 by 2 m wide. At most sites, the soil pit depth was 2 m (3 m at Alaskan sites) or bedrock, whichever was shallower. A three-sided trench shield was placed in the pit to protect personnel in the pit from collapses, and soil samples were collected from the open side.

A USDA–NRCS soil scientist familiar with local soils performed a detailed description of the soil profile to classify the soil horizons at each site (Fig. 2; more photos of soil profiles are available at data.neonscience.org/megapit-images).

Up to six intact blocks of soil were collected from different depths within the soil pit at each site. Sampling depths were chosen to capture the diversity of soil properties among the horizons. In cases where there were more than six horizons at a site, similar horizons (e.g., Bt1 and Bt2) were grouped and a single block was collected from a depth representative of both horizons. Intact soil blocks were excavated to the top of a targeted sampling depth by situating a 40- by 40-cm-wide and 16-cm-tall (25,600-cm^3) stainless steel frame (1.9 mm thick) on the soil, and then slowly excavating soil from the edge of the block (by hand, hori-hori knives, etc.) while lowering the frame around the soil block (Fig. 3A). It was evident if, when sampling, we encountered a large rock(s) and/or a large root(s) that was positioned both inside and outside of the block. If we encountered a large root, we cut the root as close to the outside of the block and kept the remainder of the root in place within the sample. If we encountered a large rock, we removed it and kept sampling down to the point where we could capture the void (left by the rock) within the sample. Once the sides of the frame completely surrounded the block, the stainless-steel bottom plate was hammered into the soil (Fig. 3B) and then the block was carefully lifted out of the soil pit. If rocks were encountered when hammering in the bottom plate, the bottom plate was moved deeper until it could be fully inserted. Once the soil block was extracted, the excess soil and rocks were removed from the bottom of the block. Any voids created by the removal of large rocks were packed with soil from the corresponding depth. Next, the top and bottom plates were strapped onto the soil block using stainless steel strapping, the block was labeled (Fig. 3C), placed in a leak-proof container, and shipped to one of the analytical laboratories.

Soil block collections began in mid-2012 and are still in progress. To date, 222 soil blocks from 40 terrestrial NEON sites have been collected, with 155 of these soil blocks from 33 sites having been analyzed. The analyzed blocks represent the majority of soil types and orders found across the continental United States (Loescher et al., 2014); soil moisture calibrations of these samples are presented here.

Soil-Specific Calibrations

The manufacturer's recommended calibration method involves installing at least six in situ soil water content profiles in the field, wetting the soil around two profiles, leaving two profiles at ambient conditions, and establishing a rainout shelter over the remaining two profiles (Sentek, 2011). Sensor readings are then taken before destructively collecting soil cores adjacent to the profiles to determine θ_g and bulk density. However, with only six sensor profiles, the calibration method results in only six points at a given depth to construct a soil-specific calibration. Although additional measurements could be added by installing more sensors and then excavating the soil around them, this results in additional destructive sampling in the study area. Additionally, it does not allow continuous calibration against reference standard measurements (e.g., gravimetric soil moisture), thus making it difficult to accurately calibrate the sensors across a range of water contents.

To generate more accurate calibrations, we developed an alternative approach based on the methods described by Weitz et al. (1997). First, we placed the metal box containing the intact soil block (see Fig. 2C) on top of 1-cm spacers in a large plastic container. The strapping and top plate were then removed from the soil block. Deionized water was slowly added to the container in 4-cm increments during a 3- to 6-h period until the water surface reached the top of the soil block. The use of the spacers allowed the water to passively enter the soil from the bottom of the block, through the perforated bottom plate of the stainless steel box, and ensured that no air was trapped in the soil block during the wet-up phase. The soil was left to soak for 72 h to ensure that it reached saturation, with additional water being added daily if the water level dropped below the top of the block. Next, the water was drained from the container, leaving the saturated soil block exposed to the ambient laboratory environment. A soil corer, with the same diameter as the EnviroSCAN tube, was inserted into the center of the soil block to remove the soil, and an EnviroSCAN installation tube was inserted vertically into the hole. If a rock or other obstacle was encountered during installation, the tube was installed as close to the middle of the block as possible. The soil block was left to drain under gravity until field capacity was reached (i.e., drainage of water from the soil block ceased). Once at field capacity, an EnviroSCAN sensor was installed in the access tube. The 40- by 40- by 16-cm soil block included buffer zones of $\geq$3 cm in all directions around the EnviroSCAN measurement zone. A 100 Ω platinum resistance thermometer (PRT) was inserted vertically into the soil at a distance of least 16 cm from the EnviroSCAN access tube and at least 5 cm from the edge of the soil block. This ensured independence to the capacitance measurement zone of the EnviroSCAN sensor and minimized artifacts due to edge effects introduced by the metal plates. The entire assembly was then placed on a 100-kg load capacity digital scale (Ohaus D51XW100WL4, Ohaus Corp.) and allowed to air dry for an extended period of time (hereafter known as *dry-down*; Fig. 4). Our calibration process aimed to quantify a continuous time series of θ_v between field capacity to near the wilting point because this represents a large portion of the θ_v range expected in the field. Once the dry-down process began, we did not disturb the soil block to mitigate

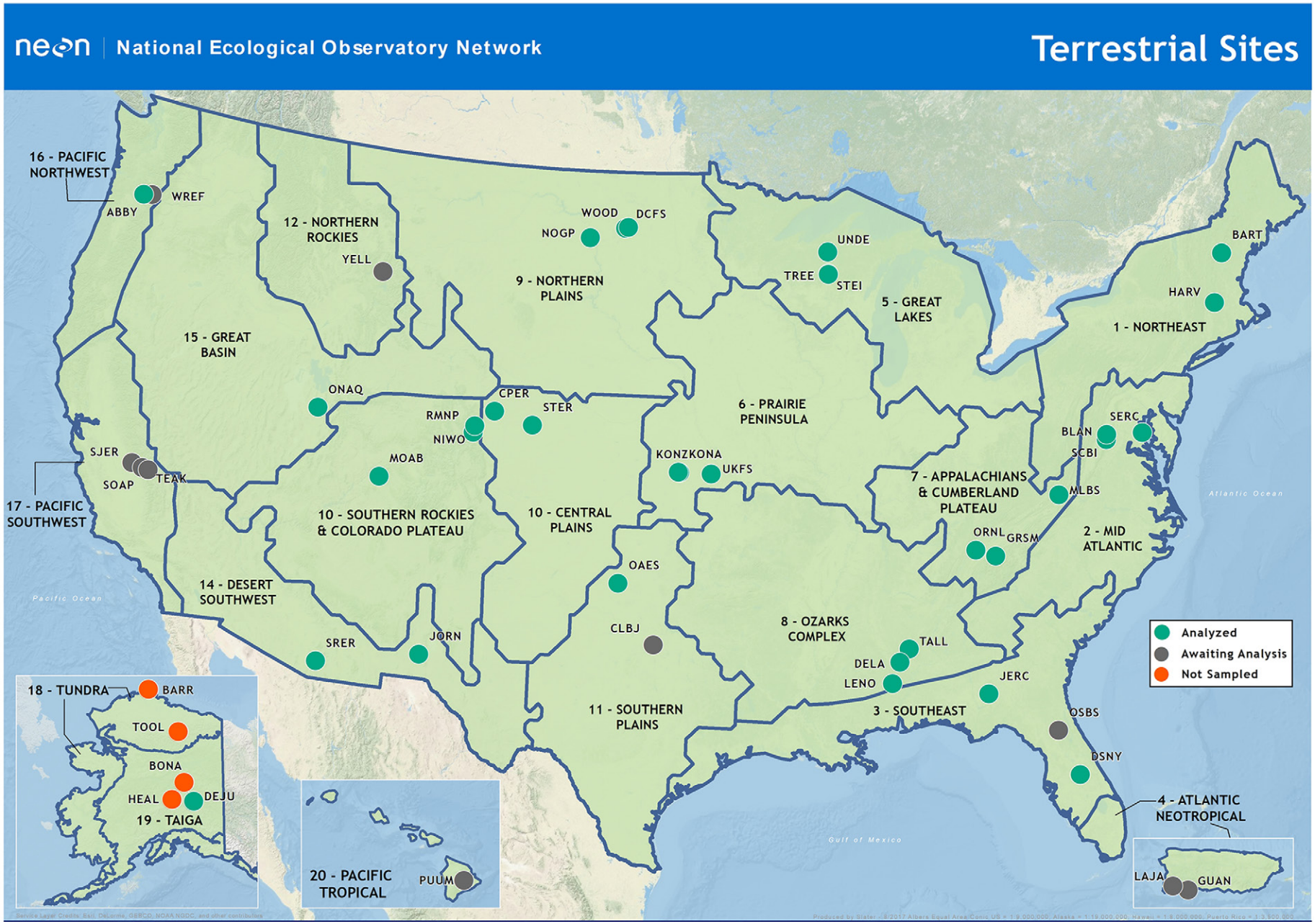

Fig. 1. Map of the National Ecological Observatory Network's terrestrial sites where soil sampling and soil-specific calibrations have been generated (green dots) or are scheduled to be generated (gray dots). Orange dots indicate sites where soil blocks will not be collected due to permit and/or land owner restrictions.

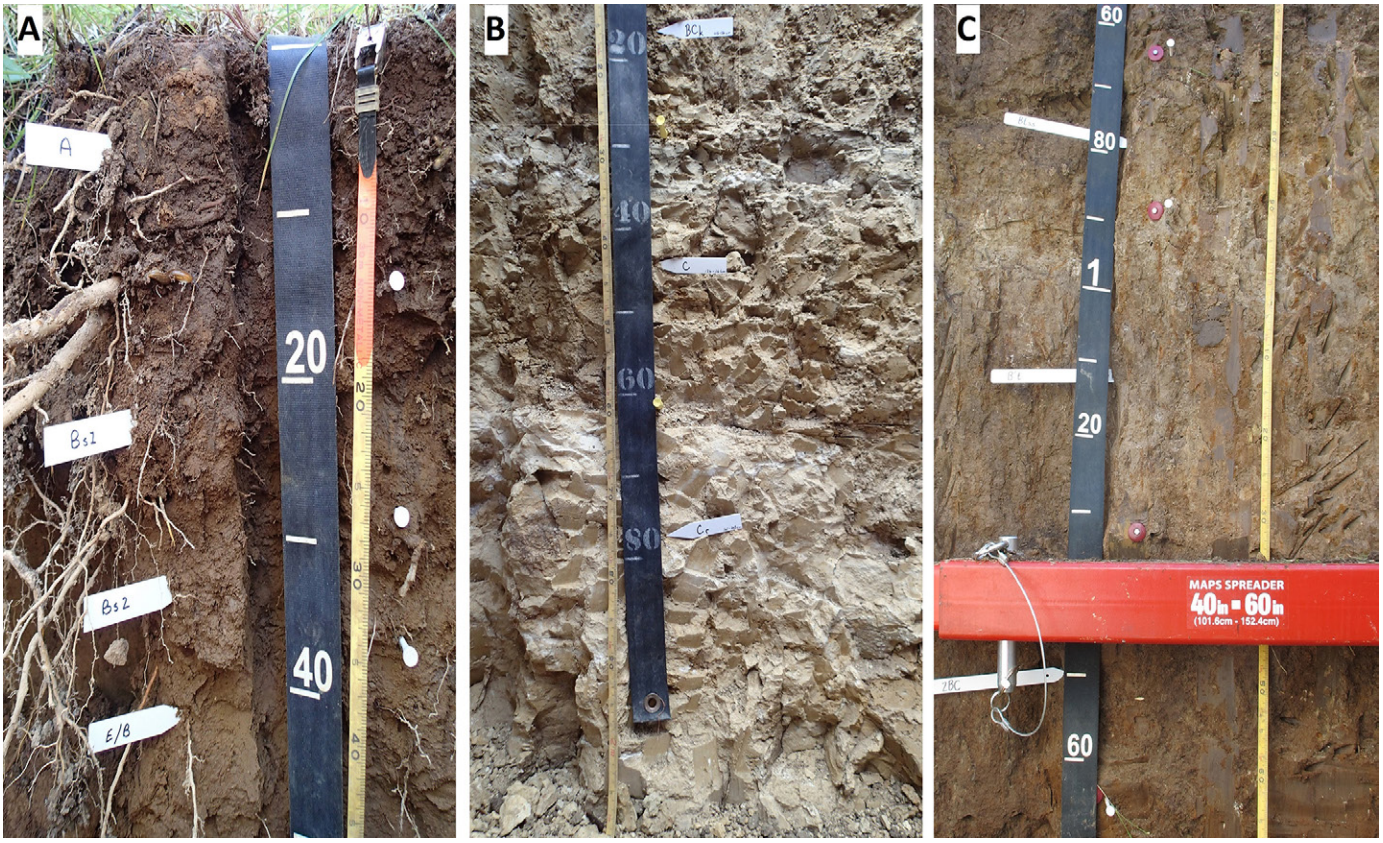

Fig. 2. Examples of partial soil profiles from the National Ecological Observatory Network soil pit prior to excavation: (A) Steigerwaldt (STEI) 0- to 50-cm depth, Spodosol; (B) Guanica Forest (GUAN) 115- to 200-cm depth, Aridisol; and (C) Konza Prairie Biological Station (KONZ) 60- to 170-cm depth, Mollisol. Full site names and geolocation information can be found in Supplemental Table S1.

vibrations, which can alter the water disposition in drying soils (Almajmaie et al., 2017). All sensors were connected to a CR1000 datalogger (Campbell Scientific), and the sensor cables were secured to minimize their influence on the recorded weight. The datalogger recorded scaled frequency and salinity (both unitless), the total weight of the assembly (kg), and the soil temperature (Ω) at 20-s intervals. Hereafter, the term *assembly* collectively represents the soil block, EnviroSCAN sensor and access tube, PRT probe, metal box (four side plates and the perforated bottom plate), plastic container, and 1-cm spacers. Dry-downs took place at two locations: the Marine Biological Laboratory, Woods Hole, MA, and the University of Alabama, Tuscaloosa. Data from the dataloggers (as .csv files) were transferred and stored in a large file storage repository at Github.com.

EnviroSCAN sensors, PRTs, and scales were calibrated prior to the dry-down process. The EnviroSCAN sensors require normalization in dry air and in deionized water to establish the minimum and maximum of the measurement range, and the sensor

Fig. 3. Depiction of the soil block sampling process: (A) soil is excavated from around the metal box while simultaneously lowering the metal box on the soil horizon(s) to be sampled; (B) once the soil block is full with sample, the bottom plate is pushed into the bottom of the soil block; (C) the top plate is strapped and taped to the side plates and bottom plate (whole box), and the soil block is ready to be shipped.

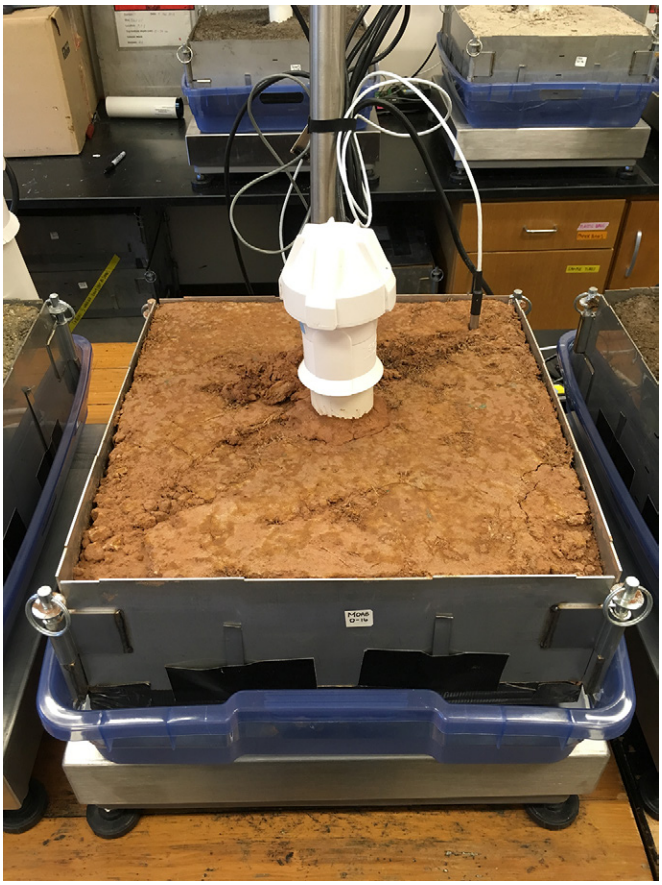

Fig. 4. Laboratory setup of the dry-down process for a soil block from the National Ecological Observatory Network's Moab site, 0- to 16-cm depth. The EnviroSCAN sensor is positioned within a tube in the center of the soil block. The platinum resistance thermometer (PRT) is inserted vertically and located in the back right corner of the soil block. The soil block is positioned on spacers (not shown) within a plastic tub and placed on a scale. The cables of the EnviroSCAN, PRT, and scale are connected to a CR1000 datalogger (not shown). The setup pictured here was identical for all calibrations.

outputs a "scaled frequency" that represents a proportion within this range (Sentek, 2011). This normalization was performed a priori in NEON's Calibration and Validation Laboratory (CVAL). The PRTs were calibrated a priori by CVAL using the triple-point method consistent with ITS-90 standards (Bedford et al., 1990; Strouse, 2008). The digital scales were calibrated prior to each dry-down using standard weights (10–100 kg, in increments of 10 kg) that met or exceeded NIST Class F specifications (National Institute of Standards and Technology, 1990).

We recognize that a vertical gradient of soil moisture existed within the soil block during the dry-down process. Given that the sensors' measurement zone spans 10 cm vertically (Sentek, 2011), the sensor was probably exposed to a range of moistures across this vertical zone. Similar gradients exist in surface soils as they dry (see Idso et al., 1974), hence the dry-down procedure was probably representative for these soils. For deeper soils, the vertical gradient of soil moisture within the soil block was probably greater than those that naturally exist when those soils are in situ. To a lesser extent, horizontal gradients in soil moisture may have also existed within the soil block during the drying process, caused by spatial variation in soil properties or preferential flow pathways. These potential discrepancies in the soil moisture of the entire block, which we determined gravimetrically, and the soil moisture of the sensor's measurement zone, are common to all soil moisture sensor calibrations where soils dry with time (see Logsdon, 2009). While this can be minimized by matching the soil block volume to the measurement zone, this increases the impact of edge effects (e.g., soil disturbance during sample collection) on the sensor's measurement zone. The size of our soil block was chosen to minimize edge effects while also making the volume as close to the sensor measurement zone as possible.

The dry-downs for the initial suite of soil blocks (n = 17) began in April 2015 and took nearly 6 mo to reach a status where the weight of the block stabilized. This indicated that further evaporation of θ_g was not possible given the laboratory conditions. It is not practical to allow each soil block 6 mo to air dry if hundreds of dry-downs are to be completed in a suitable time. As such, we amended our initial approach to be more time efficient, which included placing dehumidifiers and fans within the laboratory to reduce the relative humidity at the facility and accelerate evaporation from the soils. Periodic data collection, data uploads to the large file storage, and automated data analysis and modeling (i.e., a "data science" framework) were also completed to increase efficiency. These methods are detailed below.

Data Collection and Processing

After a soil block had been drying for at least 30 d, we downloaded the dry-down data from the large file storage and ran the data through five sequential quality control algorithms written in the R programming language v3.2.3 (R Core Team, 2016). The tests (i) removed any duplicated rows of data, (ii) removed rows where timestamps were duplicated but the measurands, e.g., soil water content, were unique from one row to another, (iii) flagged missing data and data gaps, (iv) split the bulk dataset into many smaller datasets (1/50th the temporal length of the bulk dataset), and (v) removed measurements of total assembly weight (kg) and scaled frequency measurements (unitless) that were deemed to be outliers. Outliers were identified following Tukey's (1977) approach, which makes no distributional assumptions about the data structure. Splitting the data into smaller discrete time periods prior to running Tukey's (1977) method preserved the nonlinear signature of the time series data.

Estimating Oven-Dried Soil Weight

Quantifying the oven-dried weight of the soil blocks allows absolute estimates of θ_g to be calculated. The oven-dried weights of the soil blocks could have been directly quantified by placing the soil blocks into an oven set to 105°C until the weight stabilized. However, the soil blocks used in this study were used for additional analyses following the dry-down process. Because of this, the soil blocks were not oven dried. The oven-dried weight of a given soil block was estimated using the alternative methods described here.

Data from the initial suite of soil blocks revealed that most of the soil moisture evaporated within the first 60 to 90 d (depending on soil type). An exponential decay, weight loss vs. drying time, was also present in the data. As such, asymptotes were periodically predicted by initializing R's nonlinear least squares (*nls*) function, an iterative function that produces coefficients through algorithm convergence (R Core Team, 2016) via an exponential decay equation. The asymptote served as a representation of the estimated air-dried weight of an assembly, such that

$$W_{\mathrm{TOT},t} = ab^{t} + c \quad [1]$$

where $W_{\mathrm{TOT},t}$ is the assembly weight (kg) at time t; a, b, and c are values estimated using the *nls* function; and t is the elapsed time (d) since the start of the dry-down period. The constant c represents the asymptote, i.e., the final air-dried weight (kg) of the assembly, and was initiated by setting it equal to the mean of the final 500 weight measurements within the respective dataset. Constants a and b were initialized with 10.0 and 0.9, respectively, based on preliminary testing.

The estimated weights were then used to calculate the completeness, or "proportion dried," P, of each soil block:

$$P = \frac{\overline{W}_{\mathrm{TOT,s30}} - \overline{W}_{\mathrm{TOT,f30}}}{\overline{W}_{\mathrm{TOT,s30}} - c} \quad [2]$$

where $\overline{W}_{\mathrm{TOT,s30}}$ and $\overline{W}_{\mathrm{TOT,f30}}$ are the mean assembly weights (kg) of the 30 measurements observed at the start of the dry-down period and the final 30 measurements observed prior to quantifying P, respectively. This was parameterized by dry-down data from the initial suite of soil blocks. These data were also used to determine a temporal threshold defining when the dry-down period could end without propagating large uncertainties into the final calibration. This was completed by generating truncated time series in 7-d increments starting at Day 30 (i.e., 0–30, 0–37, 0–44 d, and so on) and comparing the estimated air-dried assembly weight (c in Eq. [1]) of the truncated time series to the air-dried assembly weight of the entire time series. We considered the latter to be the "true" estimate of air-dried weight for the assembly. This allowed us to optimize the duration of the drying process, producing an accurate calibration, and estimate the uncertainty introduced by using modeled asymptotes.

Once $P \geq 90\%$ and the elapsed time of the dry-down was $\geq$72 d for an assembly, the estimated air-dry soil block weight, W_{AD} (kg), was quantified as a function of the corrected asymptote. The corrected asymptote, c_{c} (kg), accounted for the systematic bias of the modeled asymptotes that were estimated from the initial suite of soil blocks (n = 17):

$$c_{\mathrm{c}} = \left(c - W_{\mathrm{E}}\right) - \left(c - W_{\mathrm{E}}\right)Y_1 \quad [3]$$

$$W_{\mathrm{AD}} = c_{\mathrm{c}} - c_{\mathrm{c}}Y_2 \quad [4]$$

where Y_2 is an empirically derived coefficient, 0.006145 (kg), W_{E} is the collective weight (kg) of the assembly's equipment components, i.e., assembly weight minus soil block weight, and Y_1 is an empirically derived coefficient, 0.016281 (kg).

To account for the water remaining in the air-dried soil blocks and estimate the oven-dried soil block weights, we incorporated data from bulk soil samples that were collected at each horizon from the same soil pits as the soil blocks. The bulk soil samples had a volume of ~4 L (mineral horizons) or ~12 L (organic horizons) and were used to determine the 2- to 5- and 5- to 20-mm rock mass, the air-dry to oven-dry ratio of the <2-mm fraction, and a wide range of other physical and chemical properties at the NRCS Kellogg Soil Survey Laboratory (Soil Survey Staff, 2004). We calculated the oven-dry weight of the soil block using

$$W_{\mathrm{OD}} = \frac{W_{\mathrm{AD}} - \left[\left(W_{\mathrm{AD}}/16\right)\sum_{h=1}^{n} d_h\left(W_{\mathrm{R25},h} + W_{\mathrm{R520},h}\right)\right]}{\left(1/16\right)\sum_{h=1}^{n} d_h Z_{\mathrm{AO},h}} + \left[\frac{W_{\mathrm{AD}}}{16}\sum_{h=1}^{n} d_h\left(W_{R25,h} + W_{R520,h}\right)\right] \quad [5]$$

where W_{OD} is the oven-dried weight (kg) of the soil block, the number 16 represents the total depth (cm) of the soil block, and $W_{\mathrm{R25},h}$, $W_{\mathrm{R520},h}$, d_h, and $Z_{\mathrm{AO},h}$ are the weights of the 2- to 5- and 5- to 20-mm rocks (kg kg^{-1}), the absolute depth (cm), and the air-dry to oven-dry ratio (unitless) of the soil (i.e., the <2-mm fraction), respectively, of soil horizon h within the soil block. This equation assumes that rocks did not contain water and the air-dry to oven-dry ratio of the <2-mm fraction of the bulk soil samples was representative of the <2-mm fraction of the soil block.

Gravimetric soil moisture θ_{g} was then calculated as

$$\theta_{\mathrm{g,i}} = \frac{1\times10^{5}\left(W_{\mathrm{TOT},i} - W_{\mathrm{OD}} - W_{\mathrm{E}}\right)}{\rho\left(V_{\mathrm{sb}} - V_{\mathrm{x}}\right)} \quad [6]$$

where $\theta_{\mathrm{g,i}}$ is the instantaneous θ_{g} (% w/w) for a given assembly weight, $W_{\mathrm{TOT},i}$ (kg); ρ is the density of water at 20°C, 0.9982 g cm^{-3}; V_{sb} is the volume of the soil block (cm^3); and V_{x} is the collective volume of the items installed in the soil block (soil water content sensor, access tube, and PRT; cm^3). We chose to use a constant value for water density because the $\mu \pm 1\sigma$ soil temperature of the initial suite of soil blocks was 20 ± 2°C. This translates to a variance of ±1.6% (±1σ) for water density, which in turn introduces negligible uncertainty in units of cubic centimeters per cubic centimeters. It should be noted that soil temperature measurements (Ω) were converted to degrees Celcius, $T_{i,^{\circ}\mathrm{C}}$, by fitting the data to an equation traceable to first principles (Bedford et al., 1990; Strouse, 2008):

$$T_{i,^{\circ}\mathrm{C}} = k_1 T_{i,\Omega}^{2} + k_2 T_{i,\Omega} + k_3 \quad [7]$$

where $T_{i,\Omega}$ is a raw temperature measurement (Ω), and k_1, k_2, and k_3 are equal to 0.0996 °C Ω^{-2}, 235.1293 °C Ω^{-1}, and –245.2744 °C, respectively.

Soil-Specific Calibrations of Volumetric Soil Moisture Content

Soil-specific soil water content calibrations were completed by calibrating the EnviroSCAN data to the θ_g measurements. Because water molecules are more tightly held within the soil matrix as soils dry (Campbell and Norman, 1998), the rate of drying was much faster during the initial stage of the dry-down rather than toward the end. This pattern was evident in the data throughout the dry-down period. To avoid biasing the calibration equation to the dry end (because there were more data during this stage of the process), the scaled frequency and θ_g measurements were aggregated into mean values binned per 0.01 kg of total assembly weight, $W_{TOT,i}$. This produced a dataset with a uniform distribution of weight values and allowed calibration coefficients to be fit without bias. Next, θ_v values (% v/v) were generated using the EnviroSCAN sensor data and the manufacturer's default coefficients (θ_S):

$$\theta_S = \left(\frac{f_i - S_3}{S_1}\right)^{1/S_2} \quad [8]$$

where f_i is the scaled frequency as measured by the EnviroSCAN sensor during the dry-down process, and S_1, S_2, and S_3 are EnviroSCAN's factory coefficients; 0.1957, 0.404, and 0.02852, respectively (Sentek, 2011). It should be noted that the structure of Eq. [8] is internally programed in the sensor and is assumed to be the "best" fit for the EnviroSCAN's calibration. Additionally, the EnviroSCAN outputs θ_v from 0 to 100 in units of percentage by volume (Sentek, 2011). The θ_v and θ_g values were converted to cubic centimeters per cubic centimeter after the calibration process by simply dividing the volumetric percentage values by 100.

The θ_v values were then derived using the EnviroSCAN sensor data and soil-specific coefficients. To complete this task, Eq. [9] was initialized with EnviroSCAN's factory coefficients, and the soil-specific coefficients were estimated using R's *nls* function:

$$f_i = N_1\theta_{g,i}^{N_2} + N_3 \quad [9]$$

where N_1, N_2, and N_3 are the soil-specific coefficients calculated by the *nls* function. The θ_v values as predicted by the soil-specific coefficients (θ_{Ni}) were then derived via

$$\theta_{N_i} = \left(\frac{f_i - N_3}{N_1}\right)^{1/N_2} \quad [10]$$

The calibration data generated among the soil blocks showed that the EnviroSCAN-scaled frequency measurements were often less sensitive to changes in soil water content when the soils were very dry or wet, in contrast to more intermediate water content levels. This resulted in a pronounced S-shape to the calibration data for some samples (see below) that could not be produced by the EnviroSCAN equation (Eq. [8]). Hence, we repeated the calibration steps outlined in Eq. [9] and [10] with a logistic equation capable of describing the expected S-shaped relationship.

First, the logistic coefficients were estimated by the *nls* function based on EnviroSCAN-scaled frequency and θ_g:

$$f_i = \frac{L_1 - L_2}{1 + \exp\left[-L_4\left(\theta_{g,i} - L_3\right)\right]} + L_2 \quad [11]$$

where L_1, L_2, L_3, and L_4 are constants estimated by the *nls* function and were initialized with the maximum scaled frequency, minimum scaled frequency, θ_v measurement corresponding to the median scaled frequency range (all measured during the respective dry-down), and 0.1, respectively. The coefficients in the logistic equation describe various aspects of the relationship between the EnviroSCAN measurement and the true volumetric water content. Limits were placed on the minimum and maximum values for the coefficients during the *nls* fitting to ensure that implausible values were excluded (e.g., scaled frequency values outside the sensor's measurement range or moisture contents outside 0–1 $cm^3\ cm^{-3}$).

The soil-specific coefficients from Eq. [11] were then used to calculate θ_v using the logistic equation:

$$\theta_{Li} = L_3 + \frac{\log\left[\left(L_1 - L_2\right)/\left(f_i - L_2\right) - 1\right]}{-L_4} \quad [12]$$

where θ_{Li} is the individual, predicted θ_v derived using soil-specific coefficients and the logistic equation. Because the logistic equation contains both a high and low asymptote, it can occasionally predict unrealistically high and low water contents at scaled frequencies approaching L_1 and L_2. Therefore, θ_{Li} values that were <0 were replaced with 0, since θ_v must be within the range 0 to 100%. Similarly, if the measured EnviroSCAN scaled frequency was $<L_2$, V_{Li} was set to 0%, and if the measured scaled frequency was >98% of the scaled frequency range [i.e., $0.98(L_1 - L_2) + L_2$], V_{Li} was set to the largest volumetric water content gravimetrically measured during the dry-down.

For the EnviroSCAN and logistic functions, the minimum and maximum water content (θ_{Ni} and θ_{Li} from Eq. [10] and [12], respectively) for each soil block represented the range of soil moistures across which the calibration coefficients applied. Scaled frequencies that resulted in soil moistures outside this range have an unknown uncertainty.

Assigning Calibration Coefficients

It should be noted that the installation depths of soil water content sensors at NEON field sites were not known at the time of sample collection. As such, calibration coefficients from each soil block within a site were assigned to specific depth increments to create a continuous vertical profile of calibration coefficients that encompassed all possible installation depths. To do this, the depth increment of each soil horizon was assigned the calibration coefficients from the soil block that was most representative of that horizon. For example, the 2BCy soil horizon from NEON's Konza Prairie Biological Station, Kansas, was located between 132 and 164 cm below ground level and was assigned the calibration

coefficients from the soil block that was collected from 140 to 156 cm within that horizon. In some cases, the calibration coefficients from a single soil block could be assigned to two or more soil horizons. For example, calibration coefficients from a soil block collected from a Bt2 horizon might be assigned to the Bt2 and Bt3 horizons if a soil block was not collected from the Bt3 horizon. Similarly, if several thin soil horizons were present at the soil surface, they would often be assigned the calibration coefficients from the soil block that encompassed all those horizons.

Uncertainty Analysis

Uncertainty is an inevitable component of any measurement. Even with the highest degree of calibration or controlled conditions, measurement uncertainty will inherently arise to a certain extent. Below, we provide a high-level overview of uncertainty analyses followed by a breakdown of the uncertainty budget relating to calibrated estimates of θ_v. For more detailed information relating to the theories and applications of uncertainty analyses, see Joint Committee for Guides in Metrology (2008) and Csavina et al. (2017).

Overview

Broadly speaking, uncertainty estimates can be grouped into two categories: *precision* and *accuracy*. These two terms are commonly used but can sometimes infer different concepts among scientific fields (Csavina et al., 2017). To avoid confusion, we explicitly state and show (mathematically) how each is quantified throughout this study. Precision is quantified by assessing the repeatability or reproducibility of measurement. The Joint Committee for Guides in Metrology (2008) defines repeatability of measurement as the closeness of agreement between successive measurements of the same or similar objects obtained under the same conditions:

$$u(x_i) = s_i = \left[\frac{\sum_{i=1}^{n}(\bar{x}_i - x_i)^2}{n-1}\right]^{1/2} \quad [13]$$

where s_i is the unbiased, experimental standard deviation obtained from n number of independent observations x_i with mean $\bar{x}_i$. Measurement reproducibility is essentially the same as measurement repeatability, but the measurements are obtained under different conditions (e.g., changing locations or operators). Measurement repeatability is inherently captured when quantifying measurement reproducibility.

Accuracy is defined as the closeness of agreement between the result of a measurement and the true value of the measurand (Joint Committee for Guides in Metrology, 2008):

$$u(x_i) = \left[\frac{\sum_{i=1}^{n}(R_i - x_i)^2}{n-1}\right]^{1/2} \quad [14]$$

where R_i is an individual measurement of the reference standard. The result of this equation is commonly referred to as the root mean square error (RMSE). In many instances, a suite of inputs and calculations are utilized throughout a calibration process, such as was the case here. Each input inherently carries uncertainty, whether trivial or significant. The quantification and propagation of these inputs results in a combined uncertainty $u_c(y)$, which ultimately informs the validity of the overall measurement:

$$u_c(y) = \left[\sum_{i=1}^{n}\left(\frac{\partial f}{\partial x_i}\right)^2 u^2(x_i)\right]^{1/2} \quad [15]$$

where $\partial f/\partial x_i$ is the partial derivative of the function f with respect to the input quantity x_i (Joint Committee for Guides in Metrology, 2008). It should be noted that Eq. [15] assumes independence of terms.

Measurements of Gravimetric Soil Moisture Content

The ability to sample a known volume of soil directly impacts θ_g estimates (e.g., Ochsner et al., 2003; Robinson et al., 2008). Replicate bulk density samples (audit samples) were collected using a soil core sampler at a handful of sites (n = 11) across the observatory to determine the reproducibility of collecting a known volume of soil (Ayres et al., 2017). Here, we use the phrase *measurement reproducibility* to represent the collection of replicate bulk density samples because multiple soil types were collected under different conditions, e.g., different scientists and geographic locations, but the method of physically collecting the soil with the soil core sampler remained the same. The audit samples were collected at the same depths and within a few centimeters, horizontally, as the soil blocks to minimize differences resulting from the spatial heterogeneity of soil characteristics. We used the measurement reproducibility of the bulk density samples as a proxy to represent the measurement reproducibility of soil block volume. We justified this because, although it takes only a few minutes to collect a bulk density sample and can take anywhere from 1 to 8 h to collect a soil block, in both cases the goal is to collect a known volume of soil. A varying number of audit samples were taken among NEON sites. For instance, at some sites, two audit samples were collected, while at other sites, three to four audit samples were collected. As such, a pooled estimate of variance (standard deviation) s_p, based on N series of independent observations of the same variable (soil volume collected among various soil types) was used to quantify the uncertainty of the soil block volume, $u(V_{sb})$ collected from site to site:

$$u(x_i) = s_p = \left(\frac{\sum_{i=1}^{N}\nu_i s_i^2}{\sum_{i=1}^{N}\nu_i}\right)^{1/2} \quad [16]$$

where s_i is the unbiased, experimental standard deviation of the ith series of n_i independent observations (Eq. [13]) with degrees of freedom $\nu_i = n_i - 1$ (Joint Committee for Guides in Metrology, 2008). Equation [16] was also used to quantify the uncertainty of the volume of soil removed from the soil block when installing the EnviroSCAN tube.

The oven-dried weight, W_{OD}, of a soil block was a function of many inputs (see Eq. [5]). To estimate the uncertainty of the air-dried soil block weights, $u(W_{AD})$, the RMSE of the modeled air-dried weights were calculated as a function of the air-dried weights of the full time series (reference measurements) via Eq. [14]. Uncertainty estimates of the 2- to 5- and 5- to 20-mm rock weights and the air-dry to oven-dry ratio of the <2-mm fraction of each soil horizon h [$u(W_{R25,h})$, $u(W_{R520,h})$, and $u(Z_{AO,h})$, respectively] were all estimated following Eq. [16]. The absolute depth (cm) of each horizon was not assigned uncertainty bounds; this is a known, yet unquantifiable source of uncertainty. Measurement uncertainties of assembly weight, $u(W_{TOT,i})$, and equipment weight, $u(W_E)$, were derived using Eq. [13] and data from the scale's calibration procedure. Similarly, the measurement uncertainty of the calibrated PRTs was derived following Eq. [13] and was subsequently used to inform $u(\rho)$. Collectively, these uncertainties propagated to the final combined uncertainty of gravimetric water content, $u_c(\theta_g)$, which was derived following Eq. [15]. Because W_{OD} is a function of many variables, the subsequent computation of $u_c(\theta_g)$ is somewhat complex. A complete breakdown of partial derivatives and partial uncertainties relative to θ_g are provided within the R code in the supplemental material.

Measurements of Volumetric Soil Moisture Content

Estimates of θ_v produced via the EnviroSCAN are functions of scaled frequency, the respective calibration function, and measurements of the reference standard, θ_g. The reproducibility (precision) of scaled frequency measurements output by the EnviroSCAN was quantified via Eq. [13] during normalization. The fit of the respective calibration function was estimated by quantifying the RMSE of the predicted θ_v relative to θ_g (Eq. [14]). The uncertainty of the reference standard measurements was derived following the procedures detailed above. The uncertainties of each of these process components were summed in quadrature following Eq. [15] to produce a final, combined uncertainty of volumetric water contents, $u_c(\theta_v)$.

Results

At the time of this writing, 155 soil blocks from 33 NEON sites (Fig. 1; Supplemental Table S1) have been analyzed and are reported here. The time series data from the first 17 soil blocks were used to generate a consistent framework and pass–fail thresholds to make the dry down process more time efficient while ensuring a high level of calibration accuracy (see Fig. 5). We used thresholds of ≥90% dried and a duration of ≥72 d to end the dry-down for subsequent calibrations, which represented a compromise between accuracy in the calibration and elapsed time. This resulted in an average drying time of 77 d and an air-dry weight prediction uncertainty of ±0.436 kg (±1σ) for the assembly. Although the calibrations ended before the soil blocks had completely dried, the θ_g ranges observed during the dry-downs encompassed values that are typically observed in the field. Across all the soil samples, the $\mu \pm 1\sigma$ minimum and maximum θ_g were 0.071 ± 0.031 and 0.389 ± 0.084 cm^3 cm^{-3}, respectively. The full range of θ_g measured across the population of samples spanned from 0.026 to 0.590 cm^3 cm^{-3}. Since the air-dry to oven-dry ratio of the soil was always close to 1 ($\mu \pm 1\sigma$: 1.022 ± 0.016), the oven-dry weight of the block (W_{OD}) was only slightly less than the air-dry weight.

A variety of data signatures were observed when plotting θ_g measurements against raw scaled frequency measurements output by the EnviroSCAN (Fig. 6). While some of these relationships could be represented by the manufacturer's equation (e.g., Fig. 7), others could not (e.g., Fig. 7A). As a result, we developed and tested an alternative (logistic) calibration equation.

Unlike the default equation provided by Sentek, the logistic equation contains coefficients that can be used to extract useful information when estimating θ_v. The point of inflection in the logistic calibration model (L_3) represents the predicted maximum sensitivity of the sensor to a given change in θ_v. Across all soil blocks, the $\mu \pm 1\sigma$ peak sensitivity occurred at 0.143 ± 0.093 cm^3 cm^{-3}, indicating that the EnviroSCAN sensors had the maximum sensitivity to changes in θ_v at drier and intermediate ranges. In contrast,

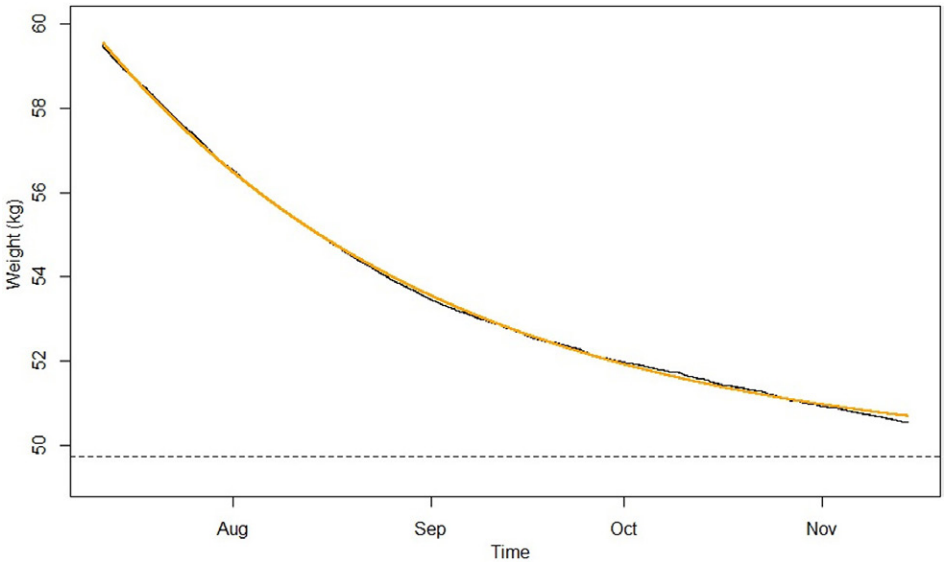

Fig. 5. Time vs. assembly weight of the of the soil block sample from the National Ecological Observatory Network's Konza Prairie Biological Station (KONZ) site, 140- to 156-cm depth. The black line represents assembly weight data passing the quality control process, the orange line represents the values predicted via Eq. [1] using R's *nls* function, and the dashed line represents the estimated, air-dry weight (c in Eq. [1]) of the assembly.

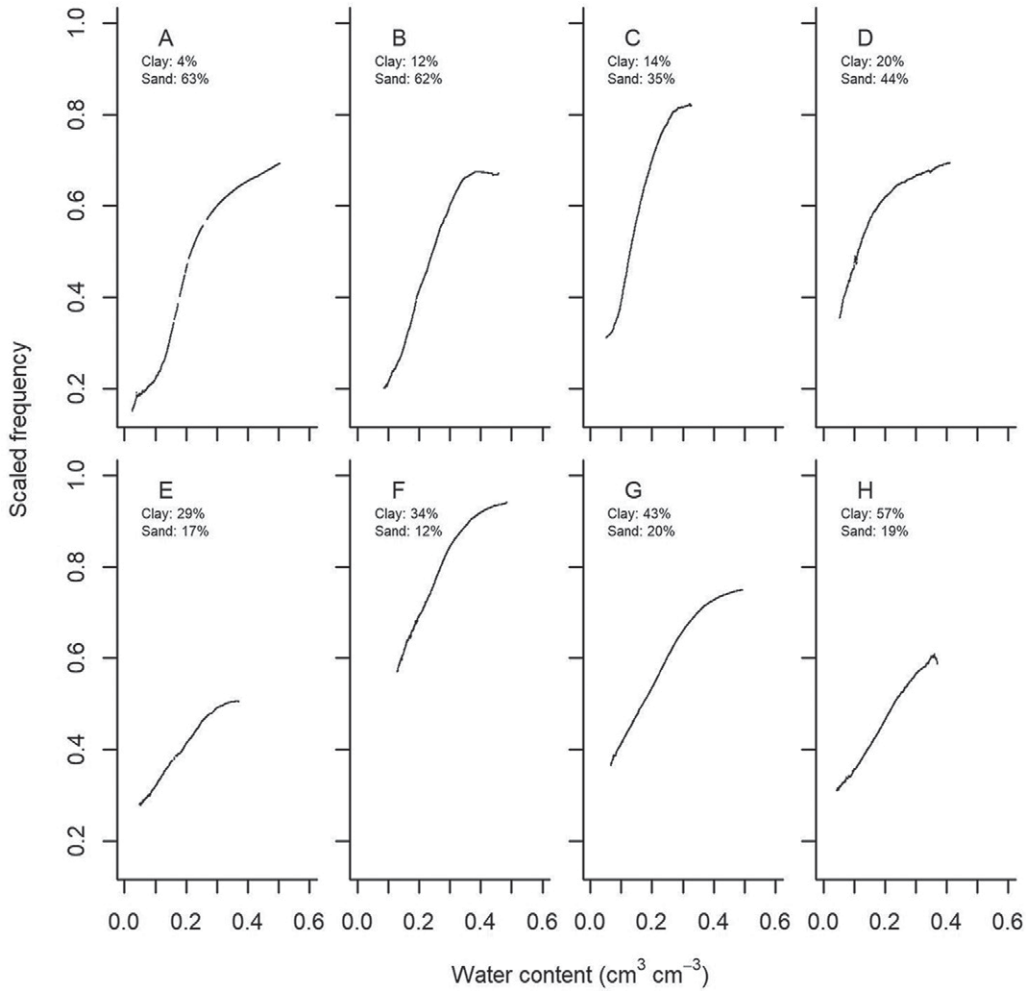

Fig. 6. Soil water content and scaled frequency relationships for example soil blocks from National Ecological Observatory Network terrestrial sites sorted by clay content: A) Bartlett Experimental Forest (BART) 08–24 cm depth; B) Smithsonian Environmental Research Center (SERC) 0–16 cm depth; C) University of Notre Dame Environmental Research Center (UNDE) 41–57 cm depth; D) Sterling (STER) 80–96 cm depth; E) Smithsonian Conservation Biology Institute (SCBI) 18–34 cm depth; F) Konza Prairie Biological Station (KONZ) 140–156 cm depth; G) Abby Road (ABBY) 51–67 cm depth; and H) Oak Ridge National Laboratory (ORNL) 75–91 cm depth. Full site names and geolocation information can be found in Supplemental Table S1.

the low and high asymptotes (L_1 and L_2, respectively) correspond to the sensor measurement thresholds predicted to be completely insensitive to changes in θ_v. We calculated the θ_v corresponding to the 10th and 90th percentile of the predicted sensor measurement range for each soil to determine the latter. Across all soil blocks, the $\mu \pm 1\sigma\ \theta_v$ corresponding to the 10th and 90th percentiles were 0.037 ± 0.072 and 0.299 ± 0.129 cm^3 cm^{-3}, respectively, indicating that the sensors were relatively insensitive to changes in θ_v in very dry and wet to very wet soil.

Thirty-one bulk density samples from 11 sites were used for the reproducibility analysis. The measurement reproducibility of these samples was found to be $\pm 5.21\%$ ($\pm 1\sigma$). We attributed all of the uncertainty in the bulk density measurements (dry weight divided by sample volume) to the volume component because the laboratory scales were calibrated to an uncertainty $\leq 0.1\%$ and we minimized differences associated with spatial variability during sample collection. This relative volumetric uncertainty translates into standard uncertainties of ± 1334 and ± 20 cm^3 (both $\pm 1\sigma$) for total soil block volume and soil volume removed during the installation of the EnviroSCAN access tube, respectively.

Use of the EnviroSCAN function with default coefficients resulted in large systematic biases, with 91% of the soil blocks displaying negative bias and 5% displaying positive bias relative to θ_g. Only 4% of the soil blocks showed no bias, i.e., the collective, predicted θ_v values were greater than, equal to, and less than θ_g measurements for a single soil block across the calibration range. The average RMSE of calibration fit (see Eq. [14]) using the nominal equation with the default coefficients was 0.123 cm^3 cm^{-3} across the population of soil blocks. Biases were corrected by using soil-specific coefficients with the EnviroSCAN function and logistic functions, which resulted in mean calibration fit uncertainties (RMSE) of ± 0.017 and ± 0.016 cm^3 cm^{-3} (both $\pm 1\sigma$), respectively. Due to the non-normal distribution of calibration fit uncertainties, especially for the logistic function, the median

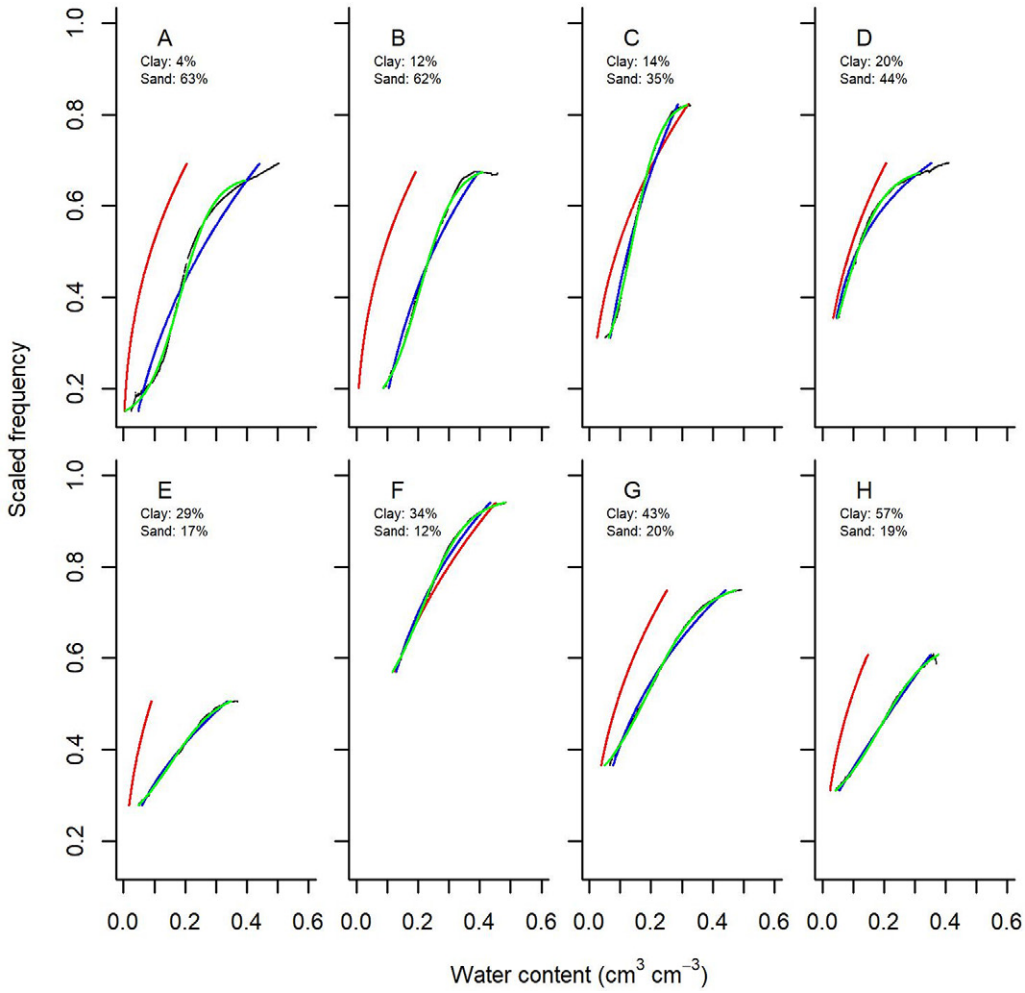

Fig. 7. Calibration fits for the soil blocks denoted in Fig. 6: raw scaled frequency (black lines); EnviroSCAN equation with nominal coefficients (red lines); EnviroSCAN equation with soil-specific coefficients (blue lines); logistic equation with soil-specific coefficients (green lines).

RMSE of the logistic function (±0.009) was substantially lower than the median RMSE of the EnviroSCAN function (±0.014). Moreover, the soil-specific logistic function was a better fit (i.e., lower mean RMSE) for 66% (n = 102) of the soil blocks, whereas the soil-specific EnviroSCAN function resulted in a better fit for 34% (n = 53) of the soil blocks.

In addition to usually having lower RMSEs, the calibrations based on the logistic function spanned a wider range of soil moistures ($\mu \pm 1\sigma$; 0.332 ± 0.079 $cm^3\ cm^{-3}$) than the soil-specific EnviroSCAN function (0.281 ± 0.068 $cm^3\ cm^{-3}$). Indeed, out of 155 soil samples, the range of soil moisture spanned by the calibration was larger for the logistic function than the EnviroSCAN function for 154 samples (99.4%). The $\mu \pm 1\sigma$ low end of the logistic and EnviroSCAN calibration range was 0.057 ± 0.032 and 0.073 ± 0.031 $cm^3\ cm^{-3}$, respectively, while the $\mu \pm 1\sigma$ high end of the logistic and EnviroSCAN calibration range was 0.389 ± 0.082 and 0.355 ± 0.081 $cm^3\ cm^{-3}$, respectively.

Among the population of soil blocks, the mean combined uncertainty of θ_v measurements was ±0.028 $cm^3\ cm^{-3}$ (±1σ) regardless of which soil-specific calibration function was used. This uncertainty was found to be heavily influenced by the uncertainty of the reference standard (θ_g) measurements. The average uncertainty of the θ_g measurements was ±0.022 $cm^3\ cm^{-3}$ among the population of soil blocks. Collectively, the uncertainties introduced by estimating the oven-dry weights (Table 1, no. 2b) and the soil block volume (Table 1, no. 2d) were the biggest contributors to the overall uncertainty of θ_g measurements. In nearly all instances, the magnitude of the θ_g uncertainty for a given soil block exceeded the magnitudes of the RMSE estimates (Table 1, no. 1). The uncertainty arising from the EnviroSCAN's reproducibility was negligible relative to the other sources of uncertainty (Table 1, no. 3).

Discussion

We developed a robust and traceable calibration approach that identifies and quantifies uncertainties associated with θ_v measurements. By examining 155 soil blocks from 33 sites that represent a range of soil types, we found the average RMSE of θ_v measurements to be 0.123 $cm^3\ cm^{-3}$ across a θ_g range of 0.026 to 0.590 $cm^3\ cm^{-3}$ when using the manufacturer's factory coefficients. This

Table 1. Uncertainty budget of example soil blocks from four National Ecological Observatory Network sites: Bartlett Experimental Forest (BART), University of Notre Dame Environmental Research Center (UNDE), Konza Prairie Biological Station (KONZ), and Oak Ridge National Laboratory (ORNL). Columns 5 through 8 display the values of each uncertainty component in units of $cm^3\ cm^{-3}$ at 1σ. There are three main components of uncertainty in this table, denoted 1 through 3 (calibration fit, θ_g, and scaled frequency) with subcomponents denoted by lowercase letters. Uncertainties propagate 'upward' to a final combined uncertainty representing the uncertainty of a volumetric soil moisture measurement outputted by the Sentek sensor (first row). Values represent mean uncertainty estimates over the calibration range.

Uncertainty source	Uncertainty component $u(x_i)$	Eq.†	$u_{x,i}(Y) \equiv \left\lvert\frac{\partial f}{\partial x_i}\right\rvert u(x_i)$‡	Uncertainty component at 1σ			
				BART (Depth: 8–24 cm)	UNDE (Depth: 41–57 cm)	KONZ (Depth: 140–156 cm)	ORNL (Depth: 75–91 cm)
				$cm^3\ cm^{-3}$			
Volumetric soil water content (θ_v), $cm^3\ cm^{-3}$ (predicted)	$u_c(\theta_v)$	[15]	n/a§	−0.176 ± 0.023¶# ±0.038†† ±0.037‡‡	±0.038¶ ±0.024†† ±0.021‡‡	+0.025 ± 0.024¶# ±0.029†† ±0.024‡‡	−0.138 ± 0.021¶# ±0.022†† ±0.021‡‡
1. Calibrated fit, $cm^3\ cm^{-3}$	$u(\theta_{RMSE})$	[14]	$u(\theta_{RMSE})$	−0.176‡ ±0.031†† ±0.029‡‡	±0.032‡ ±0.013†† ±0.004‡‡	+0.025‡ ±0.017†† ±0.004‡‡	−0.138‡ ±0.008†† ±0.004‡‡
2. Gravimetric soil water content (θ_g), $cm^3\ cm^{-3}$	$u_c(\theta_g)$	[15]	$u_c(\theta_g)$	±0.023	±0.020	±0.024	±0.021
2a. Assembly weight, kg	$u(W_{TOT,i})$	[13]	$\left\lvert\frac{\partial \theta_g}{\partial W_{TOT,i}}\right\rvert u(W_{TOT,i})$	< ±0.001	< ±0.001	< ±0.001	< ±0.001
2b. Soil block weight (oven dry), kg	$u(W_{OD})$	[14]			see 2b.1–2b.5		
2b.1. Rock weights (2–5 mm), kg	$u(W_{R25,b})$	[16]	$\left\lvert\frac{\partial \theta_g}{\partial W_{OD}}\frac{\partial W_{OD}}{\partial W_{R25,b}}\right\rvert u(W_{R25,b})$	±0.001	< ±0.001	0	< ±0.001
2b.2. Rock weights (5–20 mm), kg	$u(W_{R520,b})$	[16]	$\left\lvert\frac{\partial \theta_g}{\partial W_{OD}}\frac{\partial W_{OD}}{\partial W_{R520,b}}\right\rvert u(W_{R520,b})$	±0.002	< ±0.001	0	< ±0.001
2b.3. Absolute depth, cm	$u(d_b)$	n/a	n/a	n/a	n/a	n/a	n/a
2b.4. Air-dry/oven-dry ratio	$u(Z_{AO,b})$	[16]	$\left\lvert\frac{\partial \theta_g}{\partial W_{OD}}\frac{\partial W_{OD}}{\partial Z_{AO,b}}\right\rvert u(Z_{AO,b})$	< ±0.001	±0.001	±0.001	< ±0.001
2b.5. Soil block weight (air dry), kg	$u(W_{AD})$	[14]	$\left\lvert\frac{\partial \theta_g}{\partial W_{OD}}\frac{\partial W_{OD}}{\partial W_{AD}}\right\rvert u(W_{AD})$	±0.017	±0.017	±0.016	±0.017
2c. Equipment weight, kg	$u(W_E)$	[13]	$\left\lvert\frac{\partial \theta_g}{\partial W_E}\right\rvert u(W_E)$	< ±0.001	< ±0.001	< ±0.001	< ±0.001
2d. Soil block volume, cm^3	$u(V_{sb})$	[16]	$\left\lvert\frac{\partial \theta_g}{\partial V_{sb}}\right\rvert u(V_{sb})$	±0.014	±0.010	±0.016	±0.011
2e. Sensor volume, cm^3	$u(V_x)$	[16]	$\left\lvert\frac{\partial \theta_g}{\partial V_x}\right\rvert u(V_x)$	< ±0.001	< ±0.001	< ±0.001	< ±0.001
2f. Density of water at 20°C, kg cm^{-3}	$u(r)$	[13]	$\left\lvert\frac{\partial \theta_g}{\partial \rho}\right\rvert u(\rho)$	<< ±0.001	<< ±0.001	<< ±0.001	<< ±0.001

continued on next page

Table 1 continued from previous page.

Uncertainty source	Uncertainty component $u(x_i)$	Eq.†	$u_{x_i}(Y) \equiv \left\lvert \frac{\partial f}{\partial x_i} \right\rvert u(x_i)$‡	Uncertainty component at 1σ			
				BART (Depth: 8–24 cm)	UNDE (Depth: 41–57 cm)	KONZ (Depth: 140–156 cm)	ORNL (Depth: 75–91 cm)
3. Scaled frequency	$u(f_i)$	[13]	$\left\lvert \frac{\partial \theta_{Si}}{\partial f_i} \right\rvert u(f_i)$ ¶	<< ±0.001¶	<< ±0.001¶	<< ±0.001¶	<< ±0.001¶
			$\left\lvert \frac{\partial \theta_{Ni}}{\partial f_i} \right\rvert u(f_i)$ ††	<< ±0.001††	<< ±0.001††	<< ±0.001††	<< ±0.001††
			$\left\lvert \frac{\partial \theta_{Li}}{\partial f_i} \right\rvert u(f_i)$ ‡‡	< ±0.001‡‡	<< ±0.001‡‡	<< ±0.001‡‡	<< ±0.001‡‡

† Equation used to derive the respective uncertainty in native units of the source.
‡ Partial uncertainty used to convert the uncertainty from native units to units of cubic centimeters per cubic centimeter.
§ n/a, not available.
¶ EnviroSCAN equation with default coefficients.
# Values are presented separately because it is poor practice to propagate in quadrature the uncertainties arising from systematic effects (bias) with uncertainties arising from random effects (Joint Committee for Guides in Metrology, 2008).
†† EnviroSCAN equation with soil-specific coefficients.
‡‡ Logistic equation with soil-specific coefficients.

level of uncertainty spans the typical range of water contents that many natural and managed ecosystem soils experience (Cosh et al., 2016; Williams et al., 2009) and is comprised mainly of systematic bias. Roughly 91% (n = 141) and 5% (n = 8) of the resulting calibration curves resulted in negative and positive bias, respectively, relative to the reference standard measurements; only 4% (n = 6) of the soil blocks could be fit using the nominal coefficients without discernable bias. Our findings confirm that the use of a single set of calibration coefficients results in large systematic biases across a range of soil types that is common among other θ_v studies (e.g., Bosch, 2004; Deb et al., 2013; Seyfried and Murdock, 2004; Sharma et al., 2017) and indicate that the use of the factory coefficients is only applicable if relative soil water content measurements are needed, e.g., if the temporal pattern is primarily of interest. Hence, we do not recommend that researchers depend only on the factory coefficients, especially if the focus is to primarily estimate absolute θ_v; such data are critical in informing process-based biogeochemical models.

Similar to previous studies, we found that soil-specific calibrations are needed if accurate absolute measurements of θ_v are required (Leib et al., 2003; Seyfried and Murdock, 2004; Sharma et al., 2017; Weitz et al., 1997; Baumhardt et al., 2000). Using soil-specific coefficients in conjunction with the EnviroSCAN function, we reduced the average RMSE of the predicted θ_v measurements to ±0.017 $cm^3\ cm^{-3}$ (±1σ) across the range of soil types and θ_g values examined in this study. We also found that the RMSE of θ_v measurements could be further reduced to 0.016 $cm^3\ cm^{-3}$ (±1σ) if the EnviroSCAN equation was replaced with the logistic equation. In addition to decreasing the mean RMSE by 5%, the mean range of soil moistures across which the logistic calibrations applied was 18% larger than the range for the EnviroSCAN calibrations (0.332 vs. 0.281 $cm^3\ cm^{-3}$, respectively).

The cause of the S-shaped relationship and the reason why it is more pronounced for some soil samples is currently unclear but presumably results from an interaction between the sensor measurement technology and soil characteristics; FDR sensors are known to be sensitive to a range of factors inherent in soils as a result of their lower operating frequency (Chen and Or, 2006; Cosh et al., 2005; Seyfried and Murdock, 2004). A suite of physical and chemical properties were measured for each soil horizon collected, and preliminary analyses indicate that soil texture may influence the shape of the relationship between soil water content and scaled frequency, with soils with higher clay content having a weak tendency to have a more S-shaped relationship. This may result from the greater porosity of clay soils (Bernoux et al., 1998), which results in a larger range of water contents and may increase the chance of encountering the inflection point in the relationship. Future work will investigate the relationships between these soil characteristics and the calibration data that were generated here.

Applying the soil-specific calibration coefficients of the logistic equation, we found that the EnviroSCAN sensors were most sensitive to a given change in soil water content at dry to intermediate soil water content ranges and relatively insensitive

at very dry (<0.037 ± 0.072 cm^3 cm^{-3}) and wet to very wet (>0.299 ± 0.128 cm^3 cm^{-3}) water contents. This suggests that changes of θ_v in very dry soils and wet to very wet soils will have a larger uncertainty or may go undetected by the EnviroSCAN. This result provides a challenge to those who wish to use these sensors in soils that frequently experience these conditions.

The function that is internally stored within the EnviroSCAN sensors (Eq. [8]) limits the utility of this calibration study to post-processing of sensor data. For most soil blocks, the relationship between sensor-scaled frequency and θ_g was better represented by a logistic equation, which cannot be produced by the EnviroSCAN factory equation. We cannot rule out the possibility that an entirely different function might provide an even better fit than the logistic function derived here. The EnviroSCAN function is capable of producing measurements at an intermediate range of volumetric water contents (e.g., 0.1–0.3 cm^3 cm^{-3}) with acceptable uncertainty when soil-specific calibrations are generated but underperforms in drier soils if an inflection point in the sensor response is present. As a result, while this sensor may be suitable for measuring soil water content at some sites, it may be less suitable at other sites depending on the study aims.

The investigation of uncertainties is gaining momentum as the primary focus of many environmental studies (e.g., Loescher et al., 2006; Ocheltree and Loescher, 2007; Campbell et al., 2011; Roberti et al., 2014; Yanai et al., 2012, 2015). Quantification of measurement uncertainties informs the validity of a measurement, which allows inferences about the measurements to be made in a confident manner. In this study, we investigated all sources of known uncertainties and uncovered interesting findings. For instance, the mean uncertainty of θ_g measurements, ±0.022 cm^3 cm^{-3} (±1σ), accounted for a large percentage of the combined uncertainty of a predicted θ_v measurement. Not disclosing this type of information is a hindrance to users of θ_v sensors. Manufacturers and researchers are sometimes unclear about what type(s) of uncertainty they disseminate (Csavina et al., 2017) or assume certain applications are appropriate for their products. For example, some manufactures may only disseminate specifications informing sensor precision (i.e., repeatability or reproducibility), which in the case of the EnviroSCAN would convey that measurements output by the sensor carry relatively little uncertainty (see Table 1, no. 3). Along the same lines, many studies involving the calibrations of soil moisture sensors provide estimates of RMSE only relative to a reference standard, yet make no mention of the uncertainty of their reference standard (e.g., Bitella et al., 2014; Bosch, 2004; Cosh et al., 2005, 2016; Dong et al., 2014; Huisman et al., 2001; Ould Mohamed et al., 1997; Rowlandson et al., 2013; Sharma et al., 2017) or dismiss it as a negligible source of uncertainty (e.g., Evett, 2008). Robinson et al. (2008) noted that the most significant source of uncertainty for determining θ_g from the field may possibly be obtaining an accurate volume of soil. Of all the studies investigated for our research, we identified only two that provided a quantitative estimate of the uncertainty of their reference standard measurements. These uncertainties, which are described to be functions of repeated soil sampling of manageable volumes, i.e., <100 cm^3, are ±0.022 cm^3 cm^{-3} (Ochsner et al., 2003) and ±0.028 cm^3 cm^{-3} (Heitman et al., 2003). Evett (2008) argued that if "good practice" is exercised while collecting samples, uncertainties of θ_g measurements should be limited to <0.01 cm^3 cm^{-3}. While this may be achievable for softer soils comprising only fine roots with no or few rocks, collecting soil samples with negligible volumetric uncertainty becomes difficult in soils where rocks and/or larger roots are ubiquitous. These factors impact the reproducibility of soil sampling and ultimately the uncertainty of the reference standard used to calibrate the θ_v estimates produced by the sensor. This concept is reflected in our study, where a sample volume uncertainty of ±5.21%, when converted to units of cm^3 cm^{-3} and propagated, results in an average uncertainty of ±0.012 cm^3 cm^{-3}. Another notable source of uncertainty of our θ_g measurements resulted from estimating oven-dried soil block weights. This type of uncertainty, which was estimated to be roughly ±0.017 cm^3 cm^{-3}, is applicable only to our study and should not be considered relevant for soil moisture calibration studies that directly oven dry θ_g samples. This source of uncertainty could have been greatly mitigated had we oven dried our soil blocks immediately following the dry-down process to directly obtain an oven-dried bulk density. However, as noted above, we used the soil blocks for other analyses post dry-down. Overlooking and/or discounting the uncertainties of reference standard measurements can lead to false proclamations regarding the overall uncertainty of calibrated θ_v measurements because the full scope of an uncertainty budget goes far beyond calibration fit estimates (e.g., RMSE). These statements are meant to stress the importance of providing a fully transparent and traceable approach to uncertainty estimation, one that inherently mitigates questions about data validity and conveys important metrological concepts. For instance, a sensor cannot be calibrated to a greater accuracy than its reference standard. This is a limitation of any sensor calibration.

In this study, we identified four sources of uncertainty that we were unable to quantify: (i) the spatial variability in soil properties among the sensor installation locations at each NEON site; (ii) the impact of potential structural changes introduced to the soil block during sampling and (possibly) shipping; (iii) the impact of extreme temperatures or large temperature fluctuations on calibrated θ_v measurements; and (iv) sensitivity of the EnviroSCAN to the saline content of the soils.

Early iterations of the observatory design included up to five soil pits per terrestrial site, which would have allowed quantification of the spatial heterogeneity component of uncertainty. However, the number of pits per site was reduced from five to one because of budget and schedule constraints, which prevents a thorough quantitative assessment of spatial heterogeneity at this time. This source of uncertainty could be quantified in the future by following a method noted by Rowlandson et al. (2013), which involves collecting soil samples from multiple points (spatially) at a site and quantifying the variance of soil characteristics.

Structural changes of the soil blocks may have been introduced during sampling, shipping, and handling of the soils at the laboratories during the dry-down setup (e.g., saturating the soils and inserting the access tube). This may have caused localized changes in θ_v measurements that may not be representative of field-based θ_v measurements. We cannot rule out the possibility that this type of disruption may have introduced uncertainties with magnitudes similar to and/or greater than those quantified here. However, we also cannot rule out the possibility that any uncertainty introduced by this type of disruption was inherently captured in our calibration process.

Because laboratory temperatures were held between 20 ± 2°C ($\mu \pm 1\sigma$) for all of the dry-downs in this study, we did not directly assess the influence of large temperature fluctuations on θ_v measurements. Baumhardt et al. (2000) found that diurnal temperature swings between 15 and 35°C were closely correlated with fluctuations of θ_v measured by the EnviroSCAN; these fluctuations ranged between 0.02 and 0.04 $cm^3\ cm^{-3}$. Because a close relationship between temperature and θ_v exists, a temperature correction could be applied to the θ_v assuming that soil temperature is monitored at a short spatial distance from the θ_v measurements. These findings convey that, although the measurement uncertainties introduced by temperature fluctuations may be equal to or slightly larger than the uncertainty components quantified in this study, they can be mitigated to a magnitude that is trivial via temperature correction.

As noted by Baumhardt et al. (2000), the EnviroSCAN can produce unrealistic estimates of θ_v in saline soils. We did not specifically investigate this in our study because we did not fluctuate the salinity levels of the water used for saturating the soil block in our dry-downs. As such, we cannot speak to the extent of this sensitivity in the soils we tested. Lastly, based on our current data, we cannot quantify the uncertainty outside the range of the population of θ_g measurements that were used to generate the calibrations (0.026–0.590 $cm^3\ cm^{-3}$). This range, however, spans expected soil water contents at our sites.

Conclusions

Previous studies have presented soil-specific calibrations for capacitance sensors but only for a small number of soil types (e.g., Bosch, 2004; Baumhardt et al., 2000; Paltineanu and Starr, 1997). These studies provided important insights, but given their smaller scale they did not fully address issues that become significant when attempting to scale up the calibration of capacitance sensors to whole networks that span wide ranges of soil orders, types, and physical characteristics. We have built on the previous studies to develop a semi-automated, production process that derives θ_v measurements made by the Sentek EnviroSCAN capacitance sensor. By examining 155 soil blocks from 33 sites that represent a range of soil types, we were able to generate soil-specific calibration coefficients for θ_v with accuracies sufficient for the NEON project. While our entire approach may be unnecessary for smaller scale studies, its philosophy and traceability to uncertainty standards is highly relevant. This approach could be adopted and improved (e.g., oven drying the soil blocks) by other large θ_v monitoring networks to determine more accurate estimates of θ_g and thus soil-specific calibrations. This, accompanied with robust uncertainty estimates, provides the largest utility to all end users.

Acknowledgments

We appreciate support from numerous researchers at the field sites who assisted with selecting the location for the soil pit and other aspects of the NEON site design. In addition, we are very grateful for support from the USDA–NRCS's soil scientists, especially Larry West, Jon Hempel, Doug Wysocki, Ellis Benham, Scarlett Bailey, Rick Ferguson, Steve Monteith, and the many others who assisted with our soil pit location selection, performed soil descriptions, and analyzed soil physical and chemical properties. We send our thanks to Melissa Slater for graphics support and also to Courtney Meier, Cody Flagg, Jennifer Everhart, Julia Spencer, Holly Abercrombie, Oliver Smith, Alison Hogeboom, Mike Patterson, Rachel Krauss, and Zhunqiao Liu for additional field and laboratory support. We thank the staff of the Marine Biological Laboratory in Woods Hole, MA, for help with maneuvering and storing the large quantities of soil blocks. We acknowledge the National Science Foundation (NSF) for on-going support. NEON is a project sponsored by the NSF and managed under cooperative support agreement (EF-1029808) to Battelle. Any opinions, findings, and conclusions or recommendations expressed in this material are those of the authors and do not necessarily reflect the views of our sponsoring agencies. We wish to thank Highland Park for inspiring many a late night scientific discussion.

References

Almajmaie, A., M. Hardie, T. Acuna, and C. Birch. 2017. Evaluation of methods for determining soil aggregate stability. Soil Tillage Res. 167:39–45. doi:10.1016/j.still.2016.11.003

Ardekani, M.R.M. 2013. Off- and on-ground GPR techniques for field-scale soil moisture mapping. Geoderma 200–201:55–66. doi:10.1016/j.geoderma.2013.02.010

Ayres, E., R. Zulueta, D. Smith, and J. Roberti. 2017. TIS soil pit sampling protocol, version C. NEON.DOC.001307vC. Natl. Ecol. Obs. Network, Boulder, CO. http://data.neonscience.org/api/v0/documents/NEON.DOC.001307vC

Basinger, J.M., G.J. Kluitenberg, J.M. Ham, J.M. Frank, P.L. Barnes, and M.B. Kirkham. 2003. Laboratory evaluation of the dual-probe heat pulse method for measuring soil water content. Vadose Zone J. 2:389–399. doi:10.2136/vzj2003.3890

Battin, T.J., L.A. Kaplan, S. Findlay, C.S. Hopkinson, E. Marti, A.I. Packman, et al. 2008. Biophysical controls on organic carbon fluxes in fluvial networks. Nat. Geosci. 1:95–100. doi:10.1038/ngeo101

Baumhardt, R.L., R.J. Lascano, and S.R. Evett. 2000. Soil material, temperature, and salinity effects on calibration of multisensor capacitance probes. Soil Sci. Soc. Am. J. 64:1940–1946. doi:10.2136/sssaj2000.6461940x

Bedford R.E., G. Bonier, H. Mass, and F. Pavese. 1990. Techniques for approximating the International Temperature Scale of 1990. F-92312. Int. Bur. Weights Measures, Sèvres, France.

Bell, J.E., M.A. Palecki, C.B. Baker, W.G. Collins, J.H. Lawrimore, R.D. Leeper, et al. 2013. US Climate Reference Network soil moisture and temperature observations. J. Hydrometeorol. 14:977–988. doi:10.1175/JHM-D-12-0146.1

Bernoux, M., D. Arrouays, C. Cerri, B. Volkoff, and C. Jolivet. 1998. Bulk densities of Brazilian Amazon soils related to other soil properties. Soil Sci. Soc. Am. J. 62:743–749. doi:10.2136/sssaj1998.03615995006200030029x

Bitella, G., R. Rossi, R. Borchicchio, M. Perniola, and M. Amato. 2014. A novel low-cost open-hardware platform for monitoring soil water content and multiple soil–air–vegetation parameters. Sensors 14:19639–19659. doi:10.3390/s141019639

Blonquist, J.M., S.B. Jones, and D.A. Robinson. 2005. Standardizing characterization of electromagnetic water content sensors: 2. Evaluation of seven sensing systems. Vadose Zone J. 4:1059–1069. doi:10.2136/vzj2004.0141

Bosch, D.D. 2004. Comparison of capacitance-based soil water probes in Coastal Plain soils. Vadose Zone J. 3:1380–1389. doi:10.2136/vzj2004.1380

Burns, M.A., H.R. Barnard, R.S. Gabor, D.M. McKnight, and P.D. Brooks. 2016. Dissolved organic matter transport reflects hillslope to stream connectivity during snowmelt in a montane catchment. Water Resour. Res. 52:4905–4923. doi:10.1002/2015WR017878

Campbell, G.S., and J.M. Norman. 1998. An introduction to environmental biophysics. Springer, New York. doi:10.1007/978-1-4612-1626-1.

Campbell, J., R. Yanai, and M. Green. 2011. Estimating uncertainties in watershed studies. Eos Trans. AGU 92(26):220. doi:10.1029/2011EO260004

Chabbi, A., H.W. Loescher, M. Tye, and D. Hudnut. 2017. Integrated experimental research infrastructures as a paradigm shift to face an uncertain world. In: A. Chabbi, and H.W. Loescher, editors, Terrestrial ecosystem research infrastructures: Challenges and opportunities. CRC Press, Boca Raton, FL. p. 3–23.

Chen, Y., and D. Or. 2006. Geometrical factors and interfacial processes affecting complex dielectric permittivity of partially saturated porous media. Water Resour. Res. 42:W06423. doi:10.1029/2005WR004744

Cosh, M.H., T.J. Jackson, R. Bindlish, J.S. Famiglietti, and D. Ryu. 2005. Calibration of an impedance probe for estimation of surface soil water content over large regions. J. Hydrol. 311:49–58. doi:10.1016/j.jhydrol.2005.01.003

Cosh, M.H., T.E. Ochsner, L. McKee, J. Dong, J.B. Basara, S.R. Evett, et al. 2016. The Soil Moisture Active Passive Marena, Oklahoma, In Situ Sensor Testbed (SMAP-MOISST): Testbed design and evaluation of in situ sensors. Vadose Zone J. 15(4). doi:10.2136/vzj2015.09.0122

Csavina, J., J.A. Roberti, J.R. Taylor, and H.W. Loescher. 2017. Traceable measurements and calibration: A primer on uncertainty analysis. Ecosphere 8(2):e01683. doi:10.1002/ecs2.1683

Davidson, E.A., D.C. Nepstad, F.Y. Ishida, and P.M. Brando. 2008. Effects of an experimental drought and recovery on soil emissions of carbon dioxide, methane, nitrous oxide, and nitric oxide in a moist tropical forest. Global Change Biol. 14:2582–2590. doi:10.1111/j.1365-2486.2008.01694.x

Deb, S.K., M.K. Shulka, P. Sharma, and J.G. Mexal. 2013. Soil water depletion in irrigated mature pecans under contrasting soil textures for arid southern New Mexico. Irrig. Sci. 31:69–85. doi:10.1007/s00271-011-0293-1

Dong, J., T.E. Ochsner, M. Zreda, M.H. Cosh, and C.B. Zou. 2014. Calibration and validation of the COSMOS rover for surface soil moisture measurement. Vadose Zone J. 13(2). doi:10.2136/vzj2013.08.0148

Entekhabi, D., E.G. Njoku, P.E. O'Neill, K.H. Kellogg, W.T. Crow, W.N. Edelstein, et al. 2010. The Soil Moisture Active Passive (SMAP) mission. Proc. IEEE 98:704–716. doi:10.1109/JPROC.2010.2043918

Evett, S.R. 2008. Gravimetric and volumetric direct measurements of soil water content. In: S.R. Evett et al., editors, Field estimation of soil water content: A practical guide to methods, instrumentation, and sensor technology. IAEA-TCS-30. Int. Atomic Energy Agency, Vienna. p. 23–37.

Evett, S.R., and P. Cepuder. 2008. Capacitance sensors for use in access tubes. In: S.R. Evett et al., editors, Field estimation of soil water content: A practical guide to methods, instrumentation and sensor technology. Int. Atomic Energy Agency, Vienna. p. 73–90.

Evett, S.R., and J.L. Steiner. 1995. Precision of neutron scattering and capacitance type moisture gages based on field calibration. Soil Sci. Soc. Am. J. 59:961–968. doi:10.2136/sssaj1995.03615995005900040001x

Gardner, C.M.K., T.J. Dean, and J.D. Cooper. 1998. Soil water content measurement with a high frequency capacitance sensor. J. Agric. Eng. Res. 71:395–403. doi:10.1006/jaer.1998.0338

Gardner, C.M.K., D.A. Robinson, K. Blyth, and J.D. Cooper. 2001. Soil water content. In: K.A. Smith and C.E. Mullins, editors, Soil and environmental analysis: Physical methods. 2nd ed. Marcel Dekker, New York. p. 1–64.

Gardner, W.H. 1986. Water content. In: A. Klute, editor, Methods of soil analysis. Part 1. Physical and mineralogical methods. SSSA Book Ser. 5. SSSA and ASA, Madison, WI. p. 493–544. doi:10.2136/sssabookser5.1.2ed.c21

Heitman, J.L., J.M. Basinger, G.J. Kluitenberg, J.M. Ham, J.M. Frank, and P.L. Barnes. 2003. Field evaluation of the dual-probe heat pulse method for measuring soil water content. Vadose Zone J. 2:552–560. doi:10.2136/vzj2003.5520

Hillel, D. 1998. Environmental soil physics, Academic Press, San Diego.

Huisman, J.A., C. Sperl, W. Bouten, and J.M. Verstraten. 2001. Soil water content measurements at different scales: Accuracy of time domain reflectometry and ground-penetrating radar. J. Hydrol. 245:48–58. doi:10.1016/S0022-1694(01)00336-5

Idso, S.B., R.J. Reginato, R.D. Jackson, B.A. Kimball, and F.S. Nakayama. 1974. The three stages of drying of a field soil. Soil Sci. Soc. Am. Proc. 38:831–837. doi:10.2136/sssaj1974.03615995003800050037x

International Atomic Energy Agency. 2008. Field estimation of soil water content: A practical guide to methods, instrumentation and sensor technology. IAEA, Vienna.

IPCC. 2007. Climate models and their evaluation. In: S. Solomon et al., editors, Climate change 2007: The physical science basis. Contribution of Working Group I to the Fourth Assessment Report of the Intergovernmental Panel on Climate Change. Cambridge Univ. Press, Cambridge, UK. p. 589–662.

Joint Committee for Guides in Metrology. 2008. Evaluation of measurement data: Guide to the expression of uncertainty in measurement (GUM). Int. Org. Stand., Geneva, Switzerland.

Kaiser, K., G. Guggenberger, and L. Haumaier. 2004. Changes in dissolved lignin-derived phenols, neutral sugars, uronic acids, and amino sugars with depth in forested Haplic Arenosols and Rendzic Leptosols. Biogeochemistry 70:135–151. doi:10.1023/B:BIOG.0000049340.77963.18

Kalbitz, K., S. Solinger, J. Park, B. Michalzik, and E. Matzner. 2000. Controls on the dynamics of dissolved organic matter in soils: A review. Soil Sci. 165:277–304. doi:10.1097/00010694-200004000-00001

Kerr, Y.H., P. Waldteufel, J.P. Wigneron, S. Delwart, F. Cabot, J. Boutin, et al. 2010. The SMOS Mission: New tool for monitoring key elements of the global water cycle. Proc. IEEE 98:666–687. doi:10.1109/JPROC.2010.2043032

Koster, R.D., P.A. Dirmeyer, Z. Guo, G. Bonan, E. Chan, P. Cox, et al. 2004. Regions of strong coupling between soil moisture and precipitation. Science 305:1138–1140. doi:10.1126/science.1100217

Leib, B.G., J.D. Jabro, and G.R. Mathews. 2003. Field evaluation and performance comparison of soil moisture sensors. Soil Sci. 168:396–408. doi:10.1097/01.ss.0000075285.87447.86

Lemon, E.R. 1956. The potentialities for decreasing soil moisture evaporation loss. Soil Sci. Soc. Am. Proc. 20:120–125. doi:10.2136/sssaj1956.03615995002000010031x

Loescher, H.W., E. Ayres, P. Duffy, H. Luo, and M. Brunke. 2014. Spatial variation in soil properties among North American ecosystems and guidelines for sampling designs. PLoS One 9(1):e83216. doi:10.1371/journal.pone.0083216

Loescher, H.W., E. Kelly, and R. Lea. 2017. National Ecological Observatory Network: Beginnings, programmatic and scientific challenges, and ecological forecasting. In: A. Chabbi and H.W. Loescher, editors, Terrestrial ecosystem research infrastructures: Challenges and opportunities. CRC Press, Boca Raton, FL. p. 27–48.

Loescher, H.W., B.E. Law, L. Mahrt, D.Y. Hollinger, J. Campbell, and S.C. Wofsy. 2006. Uncertainties in, and interpretation of, carbon flux estimates using the eddy covariance technique. J. Geophys. Res. 111:D21S90. doi:10.1029/2005JD006932

Logsdon, S.D. 2009. CS616 calibration: Field versus laboratory. Soil Sci. Soc. Am. J. 73:1–6. doi:10.2136/sssaj2008.0146

National Institute of Standards and Technology. 1990. Specifications and tolerances for reference standards and field standard weights and measures: 1. Specifications and tolerances for field standard weights (NIST Class F). NIST Handbk. 105-1. US Gov. Print. Office, Washington, DC.

Ocheltree, T.O., and H.W. Loescher. 2007. Design of the AmeriFlux portable eddy-covariance system and uncertainty analysis of carbon measurements. J. Atmos. Ocean. Technol. 24:1389–1406. doi:10.1175/JTECH2064.1

Ochsner, T.E., R. Horton, and T. Ren. 2003. Use of the dual-probe heat-pulse technique to monitor soil water content in the vadose zone. Vadose Zone J. 2:572–579. doi:10.2136/vzj2003.5720

Ould Mohamed, S., P. Bertuzzi, A. Bruand, L. Raison, and L. Bruckler. 1997. Field evaluation and error analysis of soil water content measurement using the capacitance probe method. Soil Sci. Soc. Am. J. 61:399–408. doi:10.2136/sssaj1997.03615995006100020006x

Paltineanu, I.C., and J.L. Starr. 1997. Real-time soil water dynamics using multisensor capacitance probes: Laboratory calibration. Soil Sci. Soc.

Am. J. 61:1576–1585. doi:10.2136/sssaj1997.03615995006100060006x

R Core Team. 2016. R: A language and environment for statistical computing. R Found. Stat. Comput., Vienna. www.R-project.org/

Ren, T., G.J. Kluitenberg, and R. Horton. 2000. Determining soil water flux and pore water velocity by a heat pulse technique. Soil Sci. Soc. Am. J. 64:552–560. doi:10.2136/sssaj2000.642552x

Ren, T., T.E. Ochsner, R. Horton, and Z. Ju. 2003. Heat-pulse method for soil water content measurement: Influence of the specific heat of the soil solids. Soil Sci. Soc. Am. J. 67:1631–1634. doi:10.2136/sssaj2003.1631

Roberti, J.A., M.D. SanClements, H.W. Loescher, and E. Ayres. 2014. Traceable calibration performance metrics and uncertainty estimates of minirhizotron digital imagery for fine-root measurements. PLoS One 9(11):e112362. doi:10.1371/journal.pone.0112362

Robinson, D.A., C.S. Campbell, J.W. Hopmans, B.K. Hornbuckle, S.B. Jones, R. Knight, et al. 2008. Soil moisture measurement for ecological and hydrological watershed-scale observatories: A review. Vadose Zone J. 7:358–389. doi:10.2136/vzj2007.0143

Robinson, D.A., S.B. Jones, J.M. Wraith, D. Or, and S.P. Friedman. 2003. A review of advances in dielectric and electrical conductivity measurements in soil using time domain reflectometry. Vadose Zone J. 2:444–475. doi:10.2136/vzj2003.4440

Rowlandson, T.L., A.A. Berg, P.R. Bullock, E.R. Ojo, H. McNairn, G. Wiseman, and M.H. Cosh. 2013. Evaluation of several calibration procedures for a portable soil moisture sensor. J. Hydrol. 498:335–344. doi:10.1016/j.jhydrol.2013.05.021

Rundel, P.W., and J.M. Jarrell. 1989. Water in the environment. In: R.W. Pearcey et al., editors, Plant physiological ecology: Field methods and instrumentation. Kluwer Acad. Publ., Boston, MA. p. 29–56. doi:10.1007/978-94-009-2221-1_3

Schaefer, G.L., M.H. Cosh, and T.J. Jackson. 2007. The USDA Natural Resources Conservation Service Soil Climate Analysis Network (SCAN). J. Atmos. Ocean. Technol. 24:2073–2077. doi:10.1175/2007JTECHA930.1

Seneviratne, S.I., T. Corti, E.L. Davin, M. Hirschi, E.B. Jaeger, I. Lehner, et al. 2010. Investigating soil moisture–climate interactions in a changing climate: A review. Earth-Sci. Rev. 99:125–161. doi:10.1016/j.earscirev.2010.02.004.

Sentek. 2011. Calibration manual for Sentek soil moisture sensors, Version 2.0. Sentek Pty. Ltd., Stepney, SA, Australia.

Seyfried, M.S., and M.D. Murdock. 2004. Measurement of soil water content with a 50-MHz soil dielectric sensor. Soil Sci. Soc. Am. J. 68:394–403. doi:10.2136/sssaj2004.3940

Sharma, H., M.K. Shukla, P.W. Bosland, and R. Steiner. 2017. Soil moisture sensor calibration, actual evapotranspiration, and crop coefficients for drip irrigated greenhouse chile peppers. Agric. Water Manage. 179:81–91. doi:10.1016/j.agwat.2016.07.001

Soil Survey Staff. 2004. Soil survey laboratory methods manual. Soil Surv. Invest. Rep. 42. Version 4.0. Natl. Soil Surv. Lab., Lincoln, NE.

Stanford, G., and E. Epstein. 1974. Nitrogen mineralization–water relations in soils. Soil Sci. Soc. Am. J. 38:103–107. doi:10.2136/sssaj1974.03615995003800010032

Strouse, G.F. 2008. Standard platinum resistance thermometer calibrations from the Ar TP to the Ag FP. NIST Spec. Publ. 250-81. US Gov. Print. Office, Washington, DC.

Tukey, J.W. 1977. Exploratory data analysis. Addison-Wesley, Reading, MA.

Weil, R.P., and N.C. Brady. 2017. The nature and properties of soils. 15th ed. Pearson Educ., Harlow, UK.

Weitz, A.M., W.T. Grauel, M. Keller, and E. Veldkamp. 1997. Calibration of time domain reflectometry technique using undisturbed soil samples from humid tropical soils of volcanic origin. Water Resour. Res. 33:1241–1249. doi:10.1029/96WR03956

Western, A.W., R.B. Grayson, and G. Blöschl. 2002. Scaling of soil moisture: A hydrologic perspective. Annu. Rev. Earth Planet. Sci. 30:149–180. doi:10.1146/annurev.earth.30.091201.140434

Williams, C.J., J.P. McNamara, and D.G. Chandler. 2009. Controls on the temporal and spatial variability of soil moisture in a mountainous landscape: The signature of snow and complex terrain. Hydrol. Earth Syst. Sci. 13:1325–1336. doi:10.5194/hess-13-1325-2009

World Technology Evaluation Center. 2004. Sensors for environmental observatories: Report of the NSF-sponsored workshop, Seattle, WA. 30 Nov.–2 Dec. 2004. World Technol. Eval. Ctr., Baltimore, MD. www.wtec.org/seo/final/SEO_report_final.pdf.

Yanai, R.D., C.R. Levine, M.B. Green, and J.L. Campbell. 2012. Quantifying uncertainty in forest nutrient budgets. J. For. 110:448–456. doi:10.5849/jof.11-087

Yanai, R.D., N. Tokuchi, J.L. Campbell, M.B. Green, E. Matsuzaki, S.N. Laseter, et al. 2015. Sources of uncertainty in estimating stream solute export from headwater catchments at three sites. Hydrol. Processes 29:1793–1805. doi:10.1002/hyp.10265